JOURNAL OF GEOPHYSICAL RESEARCH, VOL. 99, NO. D12, PAGES 25,705–25,731, DECEMBER 20, 1994

The chemical and radiative effects of the Mount Pinatubo eruption

Douglas E. Kinnison, Keith E. Grant, Peter S. Connell, Douglas A. Rotman and Donald J. Wuebbles[1]

Lawrence Livermore National Laboratory, Livermore, California

Abstract. The eruption of Mount Pinatubo introduced large amounts of sulfur-containing particles into the stratosphere. Stratospheric ozone measured by ozonesondes and satellites is significantly lower following the June 1991 eruption and throughout 1992 and 1993. To clarify the mechanisms leading to effects on stratospheric ozone, time-dependent stratospheric aerosol and gas experiment II (SAGE II) and cryogenic limb array elaton spectrometer (CLAES) aerosol optical extinction data and SAGE II surface area density are used as parameters in a two-dimensional (2-D) zonally averaged chemical radiative transport model. The model was integrated with time from before the eruption through December 1993. The modeled impact on global ozone results from increased rates of heterogeneous reactions on sulfate aerosols and from the increased radiative heating and scattering caused by these aerosols. The model's dynamical response to changes in forcing (from changes in radiatively active trace gas concentrations and from aerosol heating) is treated in one of three ways: (1) the stratospheric temperature is perturbed, with fixed seasonal circulation, (2) the circulation is perturbed, with fixed seasonal temperature, or (3) both circulation and temperature are unperturbed, when investigating only the impact of Mount Pinatubo increased aerosol surface area density (SAD) and aerosol scattering of actinic solar radiation. When the aerosol heating is allowed to modify the temperature distribution, the maximum change calculated in equatorial column ozone is −1.6%. The calculated equatorial temperature change and peak local ozone change in October 1991 are +6 K and −4%, respectively. When aerosol heating perturbs the circulation in the model, the maximum change in equatorial column ozone is −6%. Increased heterogeneous processing on sulfate aerosols is calculated to have changed equatorial column ozone in late 1991 by −1.5%. Global column ozone in the model in 1992 and 1993 changed by −2.8% and −2.4%, respectively. The relationship of ozone-controlling processes in the lower stratosphere is altered as well; HO_x becomes the most important catalytic cycle, followed by ClO_x and NO_x. This is driven by significant changes in trace gas concentrations. In October 1991, lower stratospheric, equatorial NO_x decreased by 40%, ClO_x increased by 60%, and HO_x increased by 25%. When the effect of heterogeneous chemical processing on sulfate aerosols is combined with aerosol heating, modifying either circulation or temperature, dramatically different ozone fingerprints with time and latitude are predicted. Model-derived changes in the equatorial region in column ozone best represented the observed data when perturbed circulation was combined with heterogeneous chemical effects. However, at high latitudes, the increased ozone production from the strengthening of the mean circulation tends to cancel the heterogeneous reduction of ozone. This is not in good agreement with observed data, especially in 1992 and 1993. When the circulation is held fixed and the temperature allowed to change, and heterogeneous chemical effects are included, the equatorial ozone decrease predicted was too small for 1991. However, the mid- to high-latitude decrease in 1992 and 1993 is in better agreement with observed data.

Introduction

Volcanic eruptions can significantly impact trace gas distributions in the upper troposphere and lower stratosphere. Massive eruptions produce large quantities of sulfur dioxide (SO_2), water, and particulates. They also can inject, depending on the type of eruption, chlorine compounds. Modeling the effects of these impulsive increases in trace constituents, in order to compare the results with observations from ground and satellite measurements, provides a unique opportunity to test current multidimensional chemical-radiative transport models of the global atmosphere. Since

[1]Now at Atmospheric Science Department, University of Illinois, Urbana.

Paper number 94JD02318.
0148-0227/94/94JD-02318$05.00

these models are currently used in assessment studies for future anthropogenic emissions of trace gases [e.g., *Prather et al.*, 1992; *World Meteorological Organization (WMO)*, 1992], quantitative understanding of the accuracy of the models is essential.

In order to model volcanic impacts on stratospheric constituents for purposes of comparing to observed perturbations, several quantities must be defined. These include the nature and magnitude of the initial impulse, the development in time of the aerosol distribution and properties both radiative and chemical, and the observed atmospheric response of key variables such as temperature and ozone and other trace constituents. Below we review the existing body of information for these variables, focusing on what is known on the time period around the eruption of Mount Pinatubo. We also briefly review recent prior model studies of volcanic impact.

Several processes occur following a major volcanic eruption. Sulfur dioxide emitted from a large volcanic eruption is injected into the stratosphere where it is converted, in the presence of the hydroxyl radical, to sulfuric acid (H_2SO_4). Aerosol formation follows rapidly as a result of the low vapor pressure of H_2SO_4 at stratospheric temperatures. Increases in the concentration or surface area density of sulfate aerosols (1) provide additional sites for heterogeneous processes and (2) increase the optical thickness of the atmosphere, increasing the scattering and absorption of solar fluxes and the absorption and emission of terrestrial infrared fluxes. If the postulated heterogeneous processes occur, the catalytic reactions that affect the concentration of ozone, or their relative importance, may be modified. As aerosol optical extinction increases, changes in local heating will occur, which can alter the mean circulation or the temperature distribution or both. Strengthening the mean circulation can lift the ozone layer, causing a localized depletion. Increasing the local temperature will affect the temperature-dependent reaction rate constants, increasing the rate of reactions that destroy ozone. Changes in actinic flux will directly modify photodissociation rates, affecting ozone balance.

Laboratory studies indicate that heterogeneous processes on sulfate aerosol surfaces at stratospheric temperatures may significantly modify a mechanism of stratospheric photochemistry based solely on homogeneous processes [*Mozurkewich and Calvert*, 1988; *Tolbert et al.*, 1988; *Hanson and Ravishankara*, 1991; *Van Doren et al.*, 1991; *Burley and Johnston*, 1992a, b; *Hanson and Ravishankara*, 1993; *Molina et al.*, 1993; *Tolbert et al.*, 1993; *Hanson et al.*, 1994]. These heterogeneous reactions have the chief impact of converting NO_x ($NO + NO_2$) species efficiently to HNO_3, thereby increasing the catalytic destruction of ozone by chlorine and hydrogen radicals [*Hofmann and Solomon*, 1989; *Rodriguez et al.*, 1991; *WMO*, 1992].

Hofmann and Solomon [1989] were the first to investigate the effects that heterogeneous chemical processes occurring on background and volcanically perturbed sulfate aerosol surfaces have on ozone abundance in the lower stratosphere. They modeled the El Chichon (17.33°N, 93.2°W, 1982) eruption (prior to the eruption of Mount Pinatubo the largest eruption in the last several decades). They added reactions converting both $ClONO_2$ and N_2O_5, on the aerosols, transforming short-lived reactive nitrogen species into HNO_3, which has a longer stratospheric lifetime. With inclusion of these processes in an ambient volcanically unperturbed model atmosphere, model-derived HNO_3 profiles were increased to agree with limb infrared monitor of the stratosphere (LIMS) instrument data from the Nimbus 7 satellite. *Hofmann and Solomon* [1989] derived maximum local ozone decreases of greater than 16% at 20 km when the El Chichon radiative and chemical perturbations were included. *Brasseur et al.* [1990] also investigated the impact of heterogeneous chemistry on ozone using a modeled eruption similar in magnitude to El Chichon. They derived column ozone decreases of up to 6% at high latitudes for a 1982 atmosphere containing approximately 2.5 parts per billion by volume (ppbv) total chlorine. When they modeled the same eruption occurring for assumed trace gas boundary conditions for the year 2010, the maximum column ozone change was −12% at a total chlorine abundance of 4.5 ppbv.

To investigate the radiative effects of an El Chichon size eruption, *Michelangeli et al.* [1989], used both a one-dimensional (1-D) radiative transfer model and a 1-D chemical kinetics model. Model-derived actinic fluxes at wavelengths longward of 350 nm increased by 10% between 16 and 30 km. The total radiation within the volcanic aerosol layer decreased by 15%. These changes in actinic flux, coupled with an increase in temperature in the aerosol layer, decreased ozone by up to 7% locally.

Verdecchia et al. [1992] modeled the El Chichon aerosol cloud using a two-dimensional (2-D) chemical-radiative transport (CRT) model of the stratosphere. They accounted for the radiative effects on photodissociation rates and stratospheric temperatures in addition to heterogeneous chemistry on sulfate aerosols. Including only the radiative effects, they derived decreases in equatorial local ozone, between 20 and 25 km, of up to 6% (column change of 3%). They also concluded that the radiative effect on ozone concentration from the increased sulfate aerosols is important in both the tropics and midlatitudes.

Prather [1992] investigated the potential for a nonlinear, catastrophic loss of stratospheric ozone if the aerosol density were greatly increased following a massive eruption. With large aerosol surface area densities coupled with rapid conversion of $ClONO_2$ to HOCl and HNO_3, and with NO_x concentrations falling below a critical level, there may be regions in the atmosphere where a threshold is crossed and large local decreases in ozone would occur. Conclusions from *Prather* [1992] and the El Chichon studies mentioned above indicate the importance of increasing our understanding of lower stratospheric chemical and radiative processes, given the potential impact of large future volcanic eruptions against a background of increasing anthropogenic trace gas emissions.

On June 15, 1991, Mount Pinatubo (15.1°N, 120.4°E) erupted, producing a stratospheric aerosol cloud that was observed in the equatorial region at altitudes between 16 and 34 km [*McCormick and Veiga*, 1992]. SO_2 emissions from Mount Pinatubo were measured by the total ozone mapping spectrometer (TOMS) instrument on the Nimbus 7 satellite to be 20,000 kt, 2–3 times the amount observed after the El Chichon eruption [*Bluth et al.*, 1992]. Although the latitude distribution of Mount Pinatubo aerosol was initially equatorial, observations suggest that some material reached midlatitudes by August 1991, primarily in the lower stratosphere. Observations suggest these perturbations to the ambient background aerosol burden are expected to have produced significant chemical and radiative effects.

Observed trace gas distributions were measured before and during the Mount Pinatubo period. Satellite measurements combined with ground-based, ozonesonde, and aircraft data represent a comprehensive, if equivocal, assessment of the potential chemical change following an eruption of this magnitude. For example, column ozone measurements derived from both the Nimbus 7 TOMS and the National Oceanic and Atmospheric Administration (NOAA) 11 satellite solar backscattered ultraviolet 2 (SBUV/2) spectrometer have been reported by *Chandra* [1993]. Chandra suggest that after the effect of the quasi-biennial oscillation (QBO) has been removed, the maximum decrease in column ozone attributed to the Mount Pinatubo eruption may not be greater than 2–4%. *Schoeberl et al.* [1993] used a different method in analyzing the Nimbus 7 TOMS data, focusing on the minimum total ozone band between 12°S and 12°N. After the QBO effect was accounted for, they derived a decrease of 5–6% in column ozone. *Schoeberl et al.* [1993] attribute this decrease in ozone to local heating by the aerosols followed by vertical upwelling. *Grant et al.* [1992], using electrochemical concentrations cell (ECC) sondes data before and after the Mount Pinatubo eruption, found local decreases in tropical ozone in the lower stratosphere as great as 20%, with column reductions of about 5–8%. In later work, *Grant et al.* [1994] measured ozone concentrations with ECC sonde and with the airborne UV differential absorption lidar (DIAL) and compared these concentrations to stratospheric aerosol gas experiment II (SAGE II) climatology. *Grant et al.* [1994] also found, in September 1991, up to 29 ± 9 Dobson units (DU) (33%) tropical ozone decreases between 16 and 28 km. Smaller but not insignificant increases were found in the 28–31 km region (5.9 ± 2 DU). These peak changes in ozone in September 1991 corresponded to a column ozone decrease of 9 ± 4%. They concluded that the agreement between their data and TOMS is within experimental error.

In the spring of 1991, ozone soundings reported by *Deshler et al.* [1992a] and *Hofmann et al.* [1992] at McMurdo and south pole both measured 50% lower local ozone concentration in the 11–13 km range. The total ozone decreased by 10% over previous years. These reductions were at altitudes where depletions have not been previously observed. They suggested this additional ozone depletion is correlated to heterogeneous chemistry from increased aerosol surface area density from the Cerro Hudson (August 1991, 46°S) eruption.

In addition, *Johnston et al.* [1992], reported 40% reduction in column NO_2 in 1991 and attributed this to the conversion of N_2O_5 to HNO_3. *Koike et al.* [1994] and *Solomon et al.* [1994] also investigated observed NO_2 changes following the Mount Pinatubo eruption. Koike et al. also showed the concurrent observed change in midlatitude column HNO_3. Solomon et al. investigated high-latitude changes in NO_2 during fall and summers in 1990–1993. In both studies, model calculations were presented, and the heterogeneous conversion of N_2O_5 to HNO_3 on volcanic sulfate aerosol was discussed. *Wilson et al.* [1993] measured ClO in the northern hemisphere during the Airborne Arctic Stratospheric Experiment II (AASE II) campaign (August 20, 1991 to March 26, 1992) and found a large correlation between the ClO/Cl_y ratio and increased surface area density. ClO abundance at middle to high latitudes between October 1991 and February 1992 was higher that in previous years [*Toohey et al.*, 1993]. Midday abundances throughout this period were uniformly between 50 and 120 parts per trillion by volume (pptv) at 20 km. *Toohey et al.* [1993] ascribe this to NO_x suppression by heterogeneous reactions on sulfate aerosols enhanced by the eruption of Mount Pinatubo. They note that during this period the high-latitude ClO abundances were observed before temperatures inside the vortex fell below the polar stratospheric cloud (PSC) formation threshold. NO_x reductions during this period were measured by *Fahey et al.* [1993]. They measured in situ sulfate aerosol and total reactive nitrogen at middle latitudes, and by comparing the NO_x/NO_y ratio (where NO_y is the sum of all inorganic nitrogen species) before and after Mount Pinatubo, they confirmed the importance of aerosol surface reactions that convert NO_x to HNO_3.

Gleason et al. [1993] reported that during 1992, TOMS on the Nimbus 7 satellite measured global average total ozone to be 2–3% lower than in any earlier year observed (1979–1991). The largest decreases were between 10°S to 20°S and 10°N to 60°N. These results were confirmed by other instruments (SBUV/2 instrument on the NOAA 11 satellite, TOMS on the Russian Meteor 3 satellite, the World Standard Dobson Instrument 83, and a collection of 22 ground-based Dobson instruments). *Grant et al.* [1994] reported decreases in tropical ozone as high as 33 ± 7 DU between 4°S and 8°S from May to August 1992 that peaked in July over Brazzaville. Other studies [*Bojkov et al.*, 1993; *Kerr et al.*, 1993; and *Komhyr et al.*, 1994] also reported unusually low values throughout 1992 in the midlatitudes northern hemisphere. *Hofmann and Oltmans* [1993] reported anomalously low ozone in Antarctic region throughout 1992. On October 11 at South Pole station, total ozone reached a record low of 105 DU. They also measured anomalously low ozone in autumn 1992, before the existence of PSCs. *Solomon et al.* [1993], during the 1992 autumn period, measured elevated OClO concentration. OClO is formed from the reaction of ClO + BrO. Model results of *Solomon et al.* [1993] suggest that this large increase in OClO was from direct activation of $ClONO_2$ to ClO (from the increased stratospheric surface area density following Mount Pinatubo). *Hofmann et al.* [1994] measured ozone profiles obtained at midlatitudes in the northern hemisphere and found in the 12–22 km region, 25% lower ozone than normal during the winter and spring of 1992–1993. They suggested that the midlatitude ozone's depletion in 1992 and 1993 was from air processed at higher latitudes (although seldom ≥60°N), where colder temperatures increased chlorine-catalyzed ozone destruction. TOMS data [*Herman and Larko*, 1994] in 1993 showed ozone decreases at high latitudes of 12.5% below the 1979–1991 envelope of historical values. At midlatitudes, TOMS 1993 ozone was 7%, and at low latitudes 4%, below the historical values. In addition, area-weighted averages of the 1992–1993 TOMS data suggest that the change in ozone occurred primarily in the northern hemisphere. *Herman and Larko* [1994] reported that the global 1993 ozone amount was 3% lower than the 1979–1991 average, 5% below the historical envelope in the northern hemisphere and near the lower boundary of the historical envelope in the southern hemisphere. The microwave limb sounder (MLS) on the upper atmospheric research satellite (UARS) also observed low northern midlatitude ozone during the period of October 1992 through July 1993 [*Froidevaux et al.*, 1994]. MLS is in general agreement with TOMS, except the southern midlat-

itudes exhibit a smaller column ozone decrease in the MLS data compared to TOMS. *Froidevaux et al.* [1994] also concluded that the timing and latitudinal extent of the northern midlatitude ozone decreases are not solely related to enhanced ClO from Arctic polar processing on polar stratospheric clouds (PSCs). They believe the observed ozone reductions in 1992 and 1993 are related to both heterogeneous processes and dynamical influences (i.e., QBO).

There have been numerous theoretical studies investigating the chemical, radiative, and dynamical effects on ozone from the Mount Pinatubo eruption. *Boville et al.* [1991] investigated the dispersion of the cloud using the National Center for Atmospheric Research (NCAR) Community Climate Model (CCM2) for 180 days after the eruption. *Brasseur and Granier* [1992], *Kinnison et al.* [1992], *Pitari and Rizi* [1993], *Solomon et al.* [1993, 1994], *Wuebbles et al.* [1993], *Koike et al.* [1994], and *Rodriguez et al.* [1994] used two-dimensional CRT models in investigating the Mount Pinatubo eruption. *Kinne et al.* [1992] and *Pitari* [1993] specifically investigated the coupled radiative-dynamical perturbation following the eruption. *Bekki et al.* [1993] investigated the role of gas phase sulfur photochemistry on ozone following the eruption. Detailed comparison between approaches and conclusions of previous model studies and this work will be discussed in later sections.

In summary, there was a large number of observations that measured changes in trace gas distributions following the Mount Pinatubo eruption. Depending on the exact period, altitude, and latitude after the eruption, different mechanisms have been proposed to explain the observed changes. Comparison of the observed changes, coupled to detailed theoretical calculations, will indicate where our current understanding of stratospheric chemical, radiative, and dynamical processes is inadequate and where research is needed.

In this study, using the Lawrence Livermore National Laboratory (LLNL) 2-D zonal-averaged 2-D CRT model, the chemical and radiative effects of the Mount Pinatubo eruption are investigated. The realistic time-dependent cases included in this study focused specifically on both the radiative effects on ozone and temperature from increased aerosol extinction and the heterogeneous effects on ozone from increased surface area density (SAD). Comparison with observed data was performed to bracket and highlight the important processes that can modify temperature distributions and ozone concentrations in the stratosphere. A detailed representation of the time-dependent optical extinction was incorporated in this study, using both stratospheric aerosol and gas experiment II (SAGE II) data aboard the earth radiation budget satellite (ERBS) and cryogenic limb array etalon spectrometer (CLAES) data aboard the UARS. Lidar average profiles were used to help approximate the optical extinction in regions where the SAGE II instrument saturated (T. Deshler, personal communication, 1993). Wavelength-dependent extinction data were incorporated in this study, with extrapolation to unmeasured wavelengths based on Mie calculations. Heterogeneous processes on sulfate aerosols were treated in a time-dependent manner. $ClONO_2$ and N_2O_5 hydrolysis on sulfate aerosols were included in the chemical mechanism with reaction probabilities taken from laboratory measurements. The time-dependent SAD was derived from SAGE II by L. Thomason, NASA Langley Research Center. The SAD was corrected for saturation in the same manner as the optical extinction data.

The LLNL 2-D CRT model was integrated forward in time, initializing aerosol properties before the Mount Pinatubo eruption. Seven Mount Pinatubo perturbation were consider using the time-dependent aerosol extinction data or SAD data or both. The forcing from changes in radiatively active trace gas concentrations and aerosol heating from Mount Pinatubo is allowed to modify the model in two ways: (1) change the stratospheric temperature, with circulation seasonally fixed, and (2) change the circulation, with temperature seasonally fixed. Alternately, both circulation and temperature can be held seasonally fixed under nonvolcanic conditions. Each application of the volcanically induced forcing by aerosol and heterogeneous reactions and the model response (e.g., circulation or temperature) has a unique ozone fingerprint. Preliminary and limited versions of this study are given by *Kinnison et al.* [1992] (Quadrennial Ozone Symposium) and *Wuebbles et al.* [1993] (American Meteorological Society meeting). These studies investigated the chemical, radiative, and dynamical effects within only the first six months after the eruption. They also used a less sophisticated treatment of the radiative processes included in this study.

Two-Dimensional Model Description

The diurnal-average LLNL 2-D CRT model currently determines the atmospheric distributions of 47 chemically active atmospheric trace constituents in the troposphere and stratosphere (see *Patten et al.* [1994] for a detailed model description). The model domain extends from pole to pole and from the surface to 60 km. This version of the LLNL 2-D CRT model has a horizontal resolution of 5° in latitude, and the vertical coordinate corresponds to the logarithm of pressure, with a resolution of 1.5 km. The photochemistry represents the tropospheric and stratospheric interactions of actinic solar flux and the species families O_x, NO_y, ClO_y, HO_y, CH_4 and its oxidation products, and BrO_y. The chemical mechanism incorporates 43 transported species and four species for which abundance is determined through the assumption of instantaneous equilibrium. There are 106 thermal and 47 photolytic reactions. Source gases present in the model include NO_x, N_2O, CH_4, CO_2, CO, the chlorine-containing compounds CFC-11, CFC-12, CFC-113, CFC-114, CFC-115, HCFC-22, CCl_4, CH_3CCl_3, CH_3Cl, and the bromine-containing compounds CH_3Br, CF_2ClBr, and CF_3Br. Most of the thermal reaction rate constants were taken from the NASA Panel recommendations provided in JPL Publication 92-20 [*DeMore et al.*, 1992]. Absorption cross section information was assembled from a variety of sources, including JPL 92-20. The continuity equation for each individual species is solved using a variable time step, variable order, implicit technique for solving stiff numerical systems with strict error control.

Polar heterogeneous chemistry is present in this version of the model using climatological fields of PSCs and first-order representations of the effects of PSC heterogeneous processes on the gas phase species concentrations. These reactions are

$$ClONO_2\ (g) + HCl\ (s) \rightarrow Cl_2\ (g) + HNO_3\ (s) \quad (1)$$

$$ClONO_2\ (g) + H_2O\ (s) \rightarrow HOCl\ (g) + HNO_3\ (s) \quad (2)$$

$$HOCl\ (g) + HCl\ (s) \rightarrow Cl_2\ (g) + H_2O\ (s) \quad (3)$$

$$NO_y\ (g) \rightarrow HNO_3\ (s) \quad (4)$$

$$HNO_3\ (s) \rightarrow \text{sink (denitrification)} \quad (5)$$

Because a zonally averaged representation of temperature will not capture the existence and persistence of the regions of the stratosphere that fall below the threshold for formation of type I or type II aerosol, nitric acid trihydrate (NAT), and water ice, respectively, and because there are no continuous observations of PSC occurrence and abundance with coverage over the polar vortices, we use the frequency of occurrence of PSCs reported by the stratospheric aerosol measurement II (SAM II) instrument aboard the Nimbus 7 satellite [*WMO*, 1992, Figure 3-1]. This occultation instrument revisits the upper latitudes in both hemispheres on a regular basis throughout the winter (from about 64° at winter solstices to about 80° at spring equinoxes) and reports the presence or absence of PSC aerosol as a function of time/season and altitude. We use this map of PSC frequencies to scale proportionately the time constants applied to the PSC reactions above. For denitrification (or type II PSC formation threshold), the map in Figure 1.7.1-1 from *WMO* [1989] was also used. This map showed the envelope of minimum brightness temperature taken from the multiwave sounding unit (MSU) instrument at polar latitudes.

Among reactions (1)–(4) the time constants are assigned in proportion to the laboratory reaction probabilities or sticking coefficients. The assumption is that in the presence of PSCs all the HCl present will be instantly available for heterogeneous processing. The first-order frequency of reaction with any available $ClONO_2$ or HOCl, though, decreases with decreasing residual HCl. This probably underestimates the actual degree and rate of processing, although HCl values rapidly become small in the model. Denitrification (reaction (5)) in the southern polar vortex occurs at a frequency of 1/30 days scaled by the occurrence frequency of type II aerosol as predicted by temperatures falling below the type II formation threshold.

To represent the portion of the HNO_3 in the zonal average that is actually frozen out as NAT, the loss processes of gas phase HNO_3, photolysis and reaction with OH, are also scaled by a factor of (1 − PSC type I frequency of occurrence). This first-order, linearized approach cannot capture the actual situation of processing, recovery, and reprocessing that must actually occur, but it is adequate to represent the effect of polar processing on the global zonally averaged stratosphere for the purposes of this study.

A representation of heterogeneous reactions that occur on sulfate aerosols are also included. These reactions are

$$N_2O_5\ (g)\ [+H_2O \text{ in aerosol}] \rightarrow 2HNO_3\ (g) \quad (6)$$

$$ClONO_2\ (g)\ [+H_2O \text{ in aerosol}] \rightarrow HNO_3\ (g) + HOCl\ (g) \quad (7)$$

A complete self-consistent treatment of these reactions would require an aerosol microphysical model, the implementation of which currently has both theoretical and practical limitations. In this study we treated these reactions using the following relationship to calculate the two rate constants for the above cases:

$$K = (V)(\gamma)(\text{surface area density}),$$

parameterized as first-order loss processes with rate constants determined by specified surface area density, collision frequency, and reaction probability. Aerosol surface area density (in square microns per cubic centimeter) for the reference atmosphere is based on analysis of SAGE II data by L. R. Poole, L. W. Thomason, and G. K. Yue [*WMO*, 1992]. This distribution is representative of an atmosphere that has not been influenced by a major volcanic eruption. The surface area density distribution varies over altitude (12–32 km), latitude (90°N–90°S), and time. The effective collision velocity (V) was fixed at 5200 cm s^{-1} for this study for both species. This is close to the collision theory value for both molecules and does not vary significantly over the small temperature range over which stratospheric aerosol is found. The reaction probability per collision (γ) is based on laboratory measurements. For N_2O_5 on sulfate aerosols the reaction probability (γ_6) is set to 0.1 and is not temperature dependent [*WMO*, 1992]. The reaction probability for $ClONO_2$ on sulfate aerosols [*Hanson et al.*, 1994] is expressed by

$$\gamma_7 = 10^{(1.86-0.0747W)}$$

where W is the weight percent of the sulfate aerosol defined as

$$W = [T(0.6246Z - 14.458) + 3565] \cdot [T(-0.19988) + 1.3204Z + 44.777],^{-1}$$

T is temperature, and Z is the natural logarithm of the H_2O partial pressure in millibars.

Results and Discussion

In this section, eight different cases are considered and discussed (cases A–H, Table 1). Case A is the reference atmosphere. Here both the SAD and optical extinction data are representative of a 1990 atmosphere unperturbed by a major volcanic eruption. Change in heating rates from increased aerosol optical extinction can modify temperature, holding circulation seasonally fixed (case B), or can modify circulation, holding temperature seasonally fixed (case C). Case D investigates the effect of scattering from volcanic aerosols on photolysis rates. Here the circulation and temperature are held seasonally fixed. Case E investigates the effect of heterogeneous reactions on volcanically enhanced sulfate aerosols. The circulation and temperature are seasonally fixed. Case F also investigates the effect of volcanically enhanced heterogeneous reactions but with double the SAD. Case G is a combination of case B and case E (temperature is varied). Case H is a combination of case E and case C (circulation is varied). For the cases which included changes in either aerosol SAD, aerosol optical extinctions, or both, the model was integrated from December 22, 1990, through December 22, 1993. This section is divided into three parts which discuss (1) the radiative effects on ozone, temperature, and dynamics from a time-dependent change in the aerosol optical extinction, (2) the heterogeneous chemical effects on ozone, NO_2, and other

Table 1. Scenarios Used to Represent the Chemical, Radiative, and Dynamical Coupling From the Mount Pinatubo Eruption

Case	Ambient SAD*	Ambient Aerosol Optical Extinction†	Pinatubo SAD‡	Pinatubo Aerosol Optical Extinction§	Change in Heating Rates Into Temperature‖	Change in Heating Rates Into Dynamics‖
A¶	yes	yes	...	...	...	yes
B	yes	...	...	yes	yes	...
C	yes	...	...	yes	...	yes
D**	yes	...	...	yes	...	...
E	...	yes	yes	...	...	...
F††	...	yes	yes	...	...	...
G	...	...	yes	yes	yes	...
H	...	...	yes	yes	...	yes

"Yes" means included in scenario.

*Surface area density (SAD) for an ambient atmosphere derived from the stratospheric aerosol and gas experiment II (SAGE II) satellite (representative of low volcanic activity [*WMO*, 1992]).

†Optical extinction derived from the SAGE II satellite for an ambient atmosphere representative of low volcanic activity.

‡Surface area density derived from the SAGE II satellite after the eruption of Mount Pinatubo (L. Thomason, personal communication, 1993).

§Optical extinction derived from the SAGE II satellite after the eruption of Mount Pinatubo.

‖Changes in model-derived net heating rates are balanced by either a change in stratospheric temperature or circulation.

¶1990 reference atmosphere integrated until trace species are at steady state. Seasonally varying temperature is consistent with dynamics in this case.

**This case investigates the effect of scattering only from increased extinction.

††This scenario is the same as case E, except the SAD is multiplied by 2 everywhere.

trace gases from a time-dependent change in the aerosol surface area density, and (3) the combined effect of both radiative and chemical feedbacks.

Radiative Effects: Increase in Aerosol Extinction

The June 1991 eruption of Mount Pinatubo presented a rare opportunity to compare the effects predicted by atmospheric models with in situ and satellite measurements. Our modeling of the photochemical and radiative effects of this eruption required the generation of time-varying, zonally averaged, altitude- and latitude-dependent sets of aerosol optical extinctions. In the description below we focus on the observations, physical assumptions, and numerical techniques we used in creating aerosol extinction data sets.

The observations from SAGE II and CLAES. The observed aerosol extinction data used in this paper are primarily from SAGE II [*Russell and McCormick*, 1989] on board ERBS and from CLAES [*Mergenthaler et al.*, 1993] on board UARS.

SAGE II retrieves vertical profiles of aerosol extinction at wavelengths of 0.385 μm, 0.453 μm, 0.525 μm, and 1.02 μm. The SAGE II profiles are asynoptic, requiring slightly over 30 days to scan a complete latitude swath. Coverage at latitudes poleward of 65° is sparse. On average, there are 15 SAGE II sunrise profiles and 15 sunset profiles retrieved per 24-hour day with 1 km vertical resolution. The sunrise and sunset measurements individually group at latitudes that vary by about 6° during 24 hours. Each group of measurements progresses to successive longitudes during a day. Profiles retrieved by SAGE II normally extend down to the tropopause. However, following the eruption of Mount Pinatubo, observations made in regions of greatly increased optical depth saturated above the altitude of peak extinction.

CLAES observations provide coverage between latitudes of +80° and −80°. They also provide lower-latitude measurements at different times than SAGE II. The data are available already interpolated onto a regular spatial grid. CLAES measures profiles of aerosol extinction at several infrared wavelengths. On the basis of the reliability and differentiation of absorption efficiencies we used observations at 1257 cm^{-1} (7.955 μm) and 790 cm^{-1} (12.65 μm) for this analysis. Because infrared aerosol optical depths are substantially smaller than visible optical depths, CLAES did not suffer the saturation problems of SAGE II. On the other hand, reliable measurements from CLAES are not available until several months after the September 1991 UARS launch, considerably after the eruption of Mount Pinatubo. For use in calculation of solar heating rates and photolysis rates, CLAES extinction profiles must be scaled from the infrared into the UV visible. Either directly or indirectly, this requires an estimation of the particle size distribution and composition, adding an extra source of uncertainty.

Producing zonally averaged SAGE II profiles. We zonally averaged the SAGE II data by separately averaging sunrise and sunset observations taken during a UTC day (0000 to 2359). Approximately 15 SAGE II sunrise profiles and 15 sunset profiles are retrieved per 24-hour day. The sunrise and sunset measurements individually group at latitudes that vary by about 6° during 24 hours. Each group of measurements progresses to successive longitudes during a day.

Measurements for 0.385 μm were consistently missing below 13 km. These were filled in by extrapolation based on the extinctions measured at 1.02 μm, 0.525 μm, and 0.453 μm combined with a priori Mie calculations for representative size distributions. These calculations are described in more detail below.

Before averaging the profiles taken during a day, it was necessary to extend profiles down to the tropopause that had saturated at higher altitudes. To have formed zonal averages from only unsaturated profiles (if any) would have biased the averages at lower altitudes toward longitudes with lower

extinctions. A valuable basis for extending profiles would have been a set of time-varying, latitude-dependent, zonally averaged lidar profiles. Such a data set would be much more relevant to the grid cell values of global atmospheric models than are individual lidar profiles.

To obtain an estimate of a zonal average backscatter profile using the ergodic assumption [*Peixoto and Oort*, 1992] from a single lidar site requires nearly daily measurements over roughly 20 days. This is approximately the period required for an air parcel to circumnavigate the world. *DeFoor et al.* [1992], for example, noted that following the eruption of Mount Pinatubo, succeeding plume impulses were about 20 days apart. To obtain time and latitude dependence would require that daily measurements be taken over extended times and involve multiple sites at different latitudes. To the authors' knowledge, no such data set is available. It is outside the scope of our current efforts to undertake even the data analysis required. As a compromise, we extended saturated profiles using a profile shape derived from the first eigenvector of a time series of lidar profiles from Wyoming (T. Deshler, private communication, 1993). Using an average of tropical profiles taken by *DeFoor et al.* [1992] as a comparison to the Wyoming data, we varied the height of the profile peak as a function of the latitudinally dependent tropopause height. The amplitude of the profile was fit to data at the last three altitudes above the saturation altitude. After patching individual profiles, we zonally averaged the extinctions for all four of the available wavelengths for altitudes between 9 and 36 km.

Numerical techniques used for producing a merged, gridded, data set. Numerical techniques for interpolating SAGE II extinction profiles onto a regular grid and merging them with CLAES observations were drawn from linear inversion theory and statistical interpolation. We applied linear inversion methods to obtain latitudinally gridded extinction profiles from SAGE II retrievals at 30-day intervals, a time period comparable to that required for SAGE II to produce a complete latitude swath. Each inversion was based on all observed profiles in the prior 30 days. The linear inversion technique determines grid values such that, subject to a priori constraints, the values interpolated back to observations points from the retrieved grid values give the least squares deviation from the original observations. Using an inversion method of gridding provides more explicit control of numerical diffusion and of values assigned to grid points outside the range of influence of a set of observations than does straight forward interpolation.

To implement such an inversion scheme requires an algorithm for interpolating from grid points to observation points. Statistical interpolation uses predetermined spatial correlations between grid and observation points to determine an interpolation operator that will minimize the expected error in interpolating normally distributed data [*Alaka and Elvander*, 1972; *Journel*, 1989]. The spatial correlation operator we used for this analysis was calculated from the global and altitude average correlation of the log of the aerosol extinction. The correlation was determined as a function of the latitude separation between pairs of observations. Only post eruption SAGE II extinctions were used for these calculations, and observation pairs were constrained to be within 15 days of each other. A maximum correlation of 0.93 at zero separation was obtained by this process, giving an estimate of the random measurement error [*Alaka and Elvander*, 1972]. Taking the actual zero separation correlation to be unity provided an interpolation matrix with the diagonal dominance necessary for the interpolation operator to be positive definite (i.e., to have all positive eigenvalues).

The inversion scheme also requires a priori constraints to insure that the retrieval is well posed, robust to random errors in observations, and retrieves physically reasonable values outside of spatial regions constrained by observations [*Rodgers*, 1976]. SAGE II data are limited poleward of 65°, creating large regions in which constraining measurements are infrequent. In the absence of constraining observations, predicted grid point values are based on persistence of values derived for the previous time set. Where and when gridded CLAES data were available, they were used to constrain the expected grid point values in place of persistence. For this purpose, we used gridded CLAES data that we additionally zonally averaged and averaged over 30-day time intervals. A weak constraint on the magnitude of retrieved latitudinal second derivatives of log extinctions was applied to prevent small random variations in data from numerically amplifying into large adjacent grid point oscillations. This is a commonly used constraint in inversion algorithms [*Rodgers*, 1976].

Extrapolating SAGE II and CLAES extinctions to unmeasured wavelengths. There were several instances in our analyses for which we needed to extrapolate extinctions outside the range of wavelengths measured. As described above, extinctions for 0.385 μm were consistently missing from SAGE II profiles at altitudes below 13 km, even when the extinctions for 0.453 μm, 0.525 μm, and 1.02 μm were all present. In this case, the 0.385-μm extinctions were extrapolated from extinctions observed at the same altitude for the other wavelengths. In applying our final time- and latitude-dependent data set of extinctions to photolysis calculations, it was necessary to estimate extinctions at wavelengths shorter than 0.385 μm, the shortest wavelength measured. In merging infrared extinctions from CLAES with SAGE II extinctions, it was necessary to extrapolate from IR to UV visible wavelengths.

To enable the extrapolation process, we calculated the wavelength dependence for the Mie extinction of three lognormal size distributions. For all size distributions a composition of 68% H_2SO_4 was used. This composition was compatible with the results of *Granger et al.* [1993], based on improved stratospheric and mesospheric sounder (ISAMS) observations. It produced the best agreement with our own analysis of CLAES data, using the frequency distribution of the ratio of optical depths at 7.96 μm to those at 12.65 μm as a diagnostic. It was also similar to the 70% composition used by *Mergenthaler et al.* [1993] in their analysis of CLAES data.

The size distributions were chosen to be representative of observed modes for background or small volcanic aerosol, medium volcanic aerosol, and large volcanic aerosol [*Hofmann and Rosen*, 1983; *Deshler et al.*, 1992b; *Pueschel et al.*, 1992; *Thomason*, 1992; *Deshler et al.*, 1993]. The three size distributions had mode radii and standard deviation parameters of {0.07 μm, 1.8 μm}, {0.3 μm, 1.5 μm}, and {0.8 μm, 1.3 μm}, respectively. The ratio of the extinction at wavelengths between 0.2 and 20 μm to that at 1.02 μm is shown in Figure 1 for the three size distributions. In Table 2 we summarize the Mie calculations from Figure 1, as well as

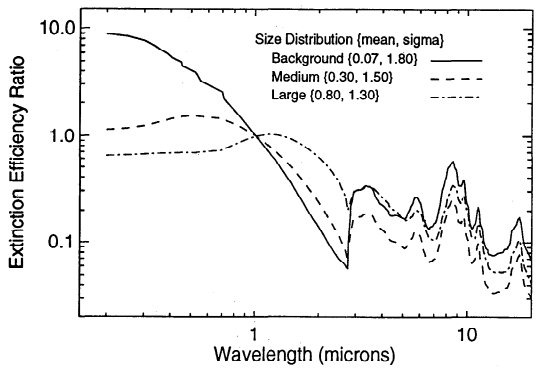

Figure 1. Wavelength dependence of aerosol extinction relative to that at 1020 nm for three lognormal size distributions. The size distributions were chosen to be representative of aerosol corresponding to background and small volcanic, medium volcanic, and large volcanic. An aerosol composition of 68% H_2SO_4 was assumed.

provide an average infrared extinction ratio. We obtained the average infrared extinctions by convolving the wavelength-dependent extinctions with a climatological estimate of the wavelength dependence of the upward flux at the tropopause. We believe this allows us to obtain reasonable estimates of aerosol effects on infrared cooling rates from a radiative transfer model in which aerosol properties are spectrally gray.

We found the range of ratios of optical depths at 0.525 μm to those at 1.02 μm, that we observed in the SAGE II data from December 1989 to May 1993, were nearly always within the range of ratios for the three size distributions above. Similarly, the distribution of ratios of optical depths at 7.96 μm to those at 12.65 μm in CLAES data from January 1992 to May 1993 data in most instances fell within the range of ratios for the three size distributions. These are indicators that the space of observed spectral extinctions can be reasonably approximated by combinations of the three size distributions.

We used the time-, latitude-, and altitude-dependent observed 0.525-μm to 1.02-μm extinction ratios as size distribution discriminators for extrapolating SAGE II observations to wavelengths shorter than 0.385 μm. These ratios were also used to estimate ratios of average infrared extinction to 1.02-μm extinction. *Thomason* [1991] had previously used the 0.525 μm to 1.02 μm ratio in empirically fitting size distributions to SAGE II data. Based on the ratios given in Table 2, the observed ratios were used to form bimodal distributions determining the wavelength dependence of the aerosol extinction. Combined with this wavelength dependence, the extinctions observed at 1.02 μm were used to scale the magnitude of the extinctions extrapolated to unmeasured wavelengths. We used the same procedure to extrapolate to 0.385 μm at low altitudes when other wavelengths were present but the 0.385-μm measurement was missing.

The wavelengths observed by CLAES range between 7.96 μm (1257 cm^{-1}) and 12.6 μm (790 cm^{-1}). Vertical profiles of infrared aerosol extinctions, in spectral regions where there is significant upward flux at the tropopause, are thus directly estimable from CLAES observations. To scale these data to UV visible wavelengths requires estimation of aerosol abundances and of aerosol size distributions. Of the wavelengths observed by CLAES, the 7.96 μm to 12.6 μm extinction ratio shows the clearest differentiation between the different size distributions discussed above. The extinction at 12.6 μm can be used as a measure of total column aerosol abundance. The ratio of the extinction at 7.96 μm to that at 12.6 μm is an estimator of the aerosol size distribution; the higher the ratio the more that smaller particles dominate the optical extinction. The extinctions at each altitude were used individually in combining CLAES observations with those from SAGE II.

Aerosol optical depths using combined SAGE II and CLAES observations. In Figure 2 we present our estimates for the zonally averaged, latitude-dependent aerosol optical depths during 1991–1993. Figure 3 shows the altitude and latitude variation in aerosol extinctions for 0.525 μm at selected times during this period. Prior to the eruption of Mount Pinatubo, retrievals in the tropics often showed higher extinctions than at middle and high latitudes. This is partly the result of an aerosol reservoir that has been observed above 20 km throughout the SAGE I and SAGE II observation periods [*Trepte and Hitchman*, 1992]. Tropical retrievals from about 15 km up to the tropopause can also be partly due to extinction by very thin cirrus (L. W. Thomason, private communication, 1993). Acting together, these factors explain the slightly higher optical depths and significantly lower 0.525 μm to 1.02 μm optical depth ratios (Figure 4) we obtain for the equatorial region as compared to higher latitudes prior to the Mount Pinatubo eruption.

In Figure 4 we present the distribution in latitude and time of the ratio of 0.525-μm optical depths to 1.02-μm optical depths. Prior to Mount Pinatubo, ratios approaching 4 were obtained at middle to high latitudes. In the tropics prior to Mount Pinatubo and nearly globally after the eruption, optical depth ratios were less than 1.2. The changes in Figure 4 following the eruption of Mount Pinatubo are seen to represent a shift from a strongly wavelength-dependent background size distribution to a much reduced wavelength dependence characteristic of medium to large aerosol. This relatively flat wavelength dependence is consistent with in situ observations by *Russell et al.* [1993a, b]. Their post-Pinatubo observations, at a number of different latitudes, display a relatively flat wavelength dependence with a consistent tendency for a slight optical depth maximum between 400 and 600 nm. These are also similar to results observed by

Table 2. Ratios of Optical Extinctions at Indicated Wavelengths Relative to Those at 1020 nm for Three Lognormal Size Distributions

	Wavelength					
Theoretical Aerosol Model	200 nm	300 nm	385 nm	453 nm	525 nm	4–20 μm Average
Background	8.89	7.78	5.94	4.49	3.90	0.13
Small volcanic	1.15	1.24	1.40	1.51	1.53	0.06
Large volcanic	0.59	0.61	0.64	0.64	0.62	0.07

The size distributions were chosen to be representative of aerosol extinction corresponding to background and small volcanic, medium volcanic, and large volcanic. An aerosol composition of 68% H_2SO_4 was assumed. The average infrared extinction between 4 and 20 μm was obtained by weighting the wavelength-dependent extinctions by an estimate of the ambient, wavelength-dependent upward flux at the tropopause.

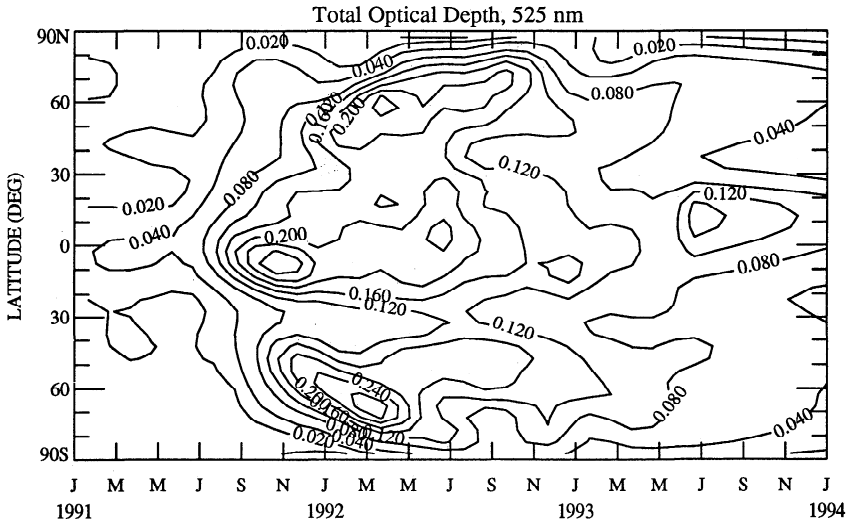

Figure 2. The latitude distribution of aerosol optical depths derived from the stratospheric aerosol and gas experiment II (SAGE II) satellite at 525 nm from 1991 through 1993.

DeLuisi et al. [1983] following the eruption of El Chichon. *Pitari and Rizi* [1993] have derived extinctions that are in reasonable agreement with our 0.525-μm results. In contrast, however, they present in their Table A1 a significantly stronger wavelength dependence than we obtain even for our background aerosol extinction calculations. Their apparent use of the wavelength dependence in their Table A1 following the eruption of Mount Pinatubo would result in their having much larger extinctions at UV wavelengths affecting photolysis than we obtain from our analyses. Manual checks of unaveraged SAGE II profiles in general confirm a relatively flat wavelength dependence.

Application of Mount Pinatubo aerosol radiative forcing. As can be seen in Figure 3, we obtained maximum equatorial aerosol extinctions in October to November 1991. Figure 5 presents the change in altitude profiles of solar, infrared, and net radiative heating rates that we obtain when we introduce mid-October 1991 extinctions into an otherwise background atmosphere. These heating rate changes are a measure of the instantaneous radiative forcing that the increased aerosol extinction represents. We obtain a peak change in the solar heating rate of 0.33 K/day at about 30 km and an infrared change of 0.27 K/day at about 25 km. The solar heating was obtained assuming a single-scattering albedo ω_0 of 0.99. This value does not come directly from Mie calculations for H_2SO_4, which yield a single-scattering albedo of unity, but is more consistent with observations [*Ogren et al.*, 1981; *Pueschel et al.*, 1992]. The choice of single-scattering albedo is important, since the solar heating scales roughly as $1 - \omega_0$. Both Ogren et al. and Pueschel et al. attribute the absorption to carbon aerosol. Lowering ω_0 to account for a carbon aerosol component is only a first-order approximation. A more accurate treatment would potentially require determination of the refractive indices and size distribution of a separate carbon aerosol as well as that of any H_2SO_4 aerosol containing dissolved carbon.

In the existing dynamical formulation of the 2-D LLNL CRT model [*Patten et al.*, 1994] we can channel changes in heating rates into changes in either temperature or circulation but not both simultaneously. We have made time-dependent calculations for both cases. Figure 6 shows the changes we obtain in local temperature (Table 1, case B) or vertical wind (Table 1, case C), comparing values for October 1991 with values from the previous year. Our results show either a 5–6 K heating (case B) in the lower equatorial stratosphere or an increase in diabatic vertical velocities (case C) of approximately 1.6 km per 100 days. *Labitzke and McCormick* [1992] observed the change in stratospheric temperature following the Mount Pinatubo eruption. Using satellite and lidar measurements, they observed the monthly averaged zonal mean 30-mbar (24 km) temperatures at 20°N in September and October, relative to the 26-year average, to be as high as 2.5 K above average, with daily mean increases at high as 3 K. Warming in the equatorial region was measured to be as high as 4 K. The LLNL 2-D CRT derived temperature perturbation (case B) slightly overestimates the observed data in the equatorial region and is in good agreement at 20°N. *DeFoor et al.* [1992], using lidar data, observed a total lift of 1.8 km, which is slightly greater than the lift per 100 days derived in this study, when all of the net heating rate change modifies the circulation (case C). In their 2-D model-derived study, *Brasseur and Granier* [1992] assumed a maximum heating rate change of 0.4 K/day in the center of the cloud which corresponds to a model-derived equatorial September 1991 temperature change of 6.8 K. In their model calculation both temperature and circulation are modified simultaneously from the assumed heating rate change. In contrast, their change in vertical circulation was roughly 2–3 times less than that derived in this study (approximately 0.5 km in 100 days). *Pitari and Rizi* [1993], also using a 2-D model, derived a change in vertical velocity that was comparable to that of *Brasseur and Granier* [1992]. *Kinne et al.* [1992] derived the heating rate change using observed aerosol data coupled to a two-stream radiative transfer model. In their 1-D approach they solved the thermodynamic equation using the model-derived heating rates and obtained vertical velocities. They derived a total lift of 1.5 km when accompanied by a heating of 0.3 K/day. Their IR heating is comparable with this study. Heating in the solar region is larger in this study (Figure 5).

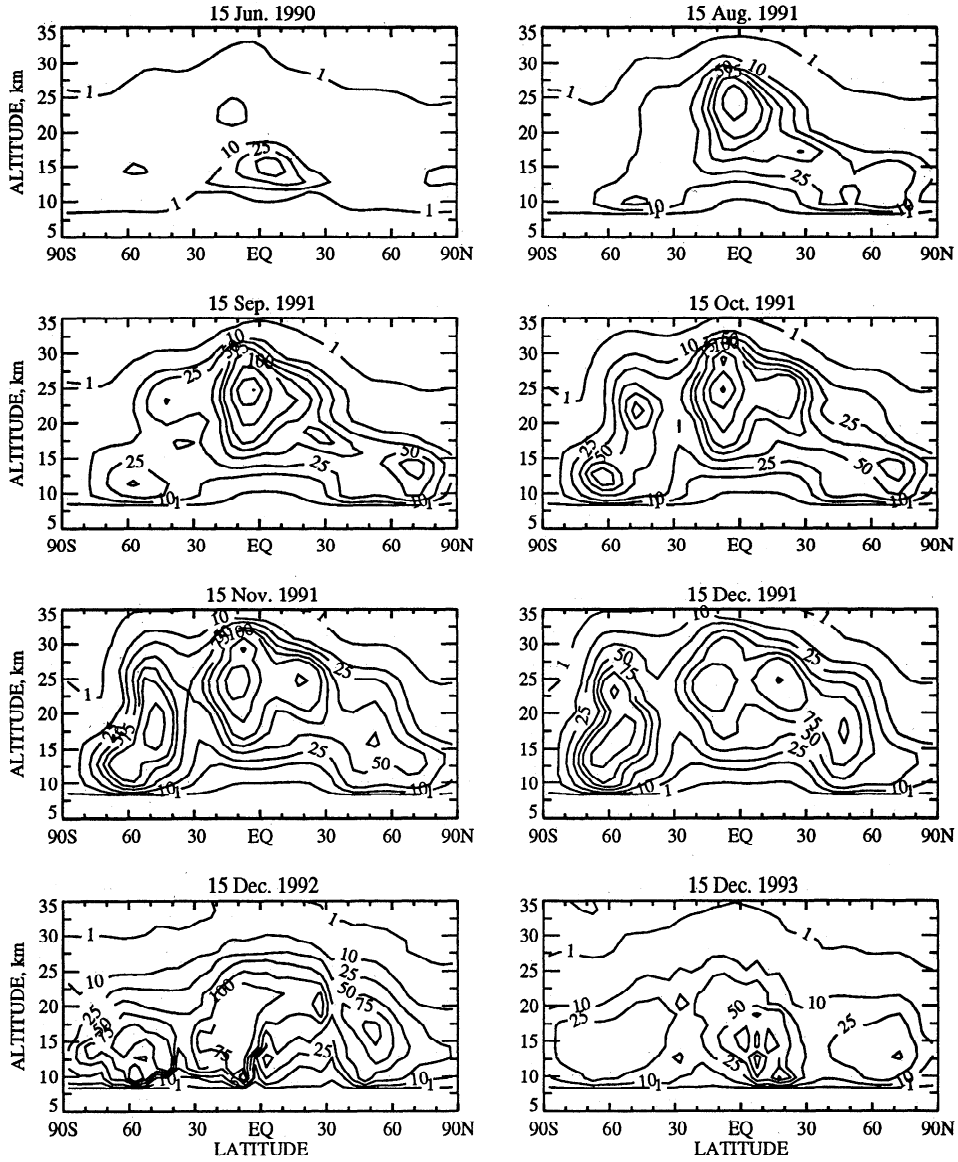

Figure 3. Latitude-altitude distributions of aerosol optical extinctions ($\times 10^{-4}$ km^{-1}) at 525 nm derived from the stratospheric aerosol and gas experiment II (SAGE II) satellite for indicated dates from June 1990 to December 1993.

As mentioned above, the solar heating is highly dependent on the choice of single-scattering albedo. *Kinne et al.* [1992] also simulated ozone concentrations using a mechanistic model which excludes horizontal mixing with the extratropics.

In Table 3, changes in equatorial column ozone (in Dobson units) from the model study of *Kinne et al.* [1992], ozonesonde data of *Grant et al.* [1994], TOMS satellite data [*Schoeberl et al.*, 1993], and this study are shown (cases B and C). The model-derived change in equatorial column ozone from *Kinne et al.* [1992] compares better with that of *Grant et al.* [1994] than it does with that of TOMS. For this study, case B, allowing only temperature to be modified, grossly underestimates the change in equatorial column ozone when compared with the observed data. For case C, when only circulation is allowed to change, the comparison is very close to TOMS and on the low end of the ozonesonde data of *Grant et al.* [1994]. There are also differences between this study and that of *Kinne et al.* [1992]. This study has a larger total heating rate change (4.8 K/day maximum) than that of *Kinne et al.* [1992]; however, the change in column ozone is less in this study (Table 3). This difference is probably due to the lack of horizontal mixing and a simpler representation of the photochemical/dynamical coupling in the *Kinne et al.* [1992] study. Case C column ozone decrease maximizes in October/November which is in good agreement with the observed data. However, this study does not show the large decrease in August as represented by the model study of *Kinne et al.* [1992] and observed data of *Grant et al.* [1994]. This study compares better to the TOMS satellite data during the August period derived by *Schoeberl et al.* [1993]. In Figures 7 and 8 the change in both local ozone and column ozone, respectively, is shown for all the cases (except case D) in Table 1. For cases B and C the maximum local equatorial ozone change (Figure 7) on October 15 is −4% and −15% respectively. Both of these model-derived changes underestimate the local equatorial

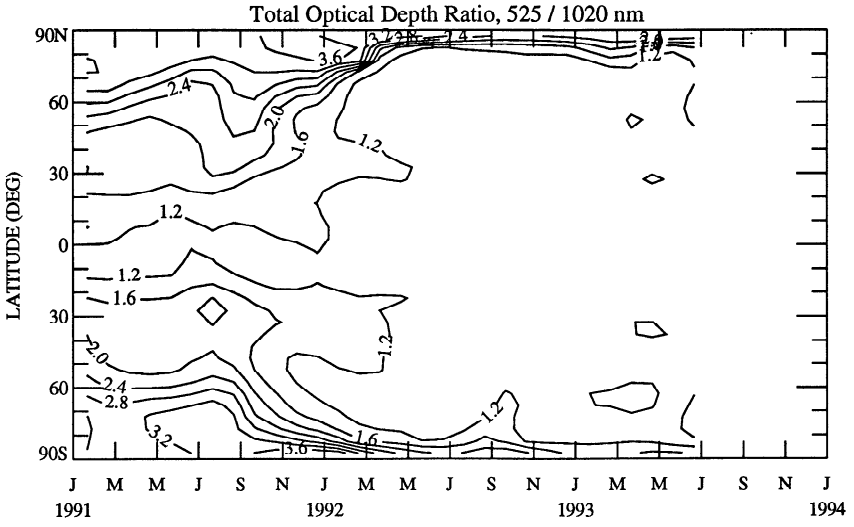

Figure 4. Time-dependent ratio of 525 nm to 1020 nm aerosol extinction derived from the stratospheric aerosol and gas experiment II (SAGE II) satellite.

ozone change (approaching −30%) observed by *Grant et al.* [1994]. Model-derived maximum equatorial column ozone (Figure 8) during the same period is slightly greater than −1% for case B and between −5% and −6% for case C. The peak change in equatorial column ozone for case C corresponds closely to the peak change in total optical depth (TOD) (Figure 2). The seasonal shape of the equatorial column ozone change is similar to that shown by both *Gleason et al.* [1993] and *Herman and Larko* [1994], with relatively large decreases in 1991 (Figure 9).

In Table 4 the model-derived average change in column ozone is divided into six regions: global (GL), northern hemisphere (NH), southern hemisphere (SH), 65°S–65°N (typical of a TOMS global average), 12°S–12°N, and 30°N–60°N. For case B the maximum change in column ozone is in the equatorial region (−1.3%, 1992). The GL, NH, and SH averages are relatively uniform in 1992 and 1993. As mentioned above, ozone change from case B is less than that derived with TOMS data reported by both *Gleason et al.* [1993] and *Herman and Larko* [1994]. When the circulation is allowed to vary (case C), the model agreement with the TOMS studies is consistent in the equatorial region for 1991 but departs at middle to high latitudes. Extratropical ozone increases from increasing the strength of the mean circulation maximize in 1992 increasing high-latitude ozone by +6% (>60°S and >60°N in 1992, Figure 8). This is partially consistent with *Pitari and Rizi* [1993]. They found similar increases (+5%) in high-latitude ozone; however, they did not see a sizable decrease in the equatorial region that would be consistent with the model studies of *Brasseur and Granier* [1992], *Kinne et al.* [1992], and this study. Globally, case C shows a net increase in ozone (+1.4%, 1992) when only the effect of aerosol heating is considered. Model-derived mid-latitude change is +3.4% between 30°N and 60°N. This has not been documented in the observed data. Increases, as mentioned above, may not be realistic and probably result from a breakdown in the zonal average dynamical representation of a 2-D model. A better arbiter of aerosol heating effects on chemical constituents like ozone would be near-future three-dimensional (3-D) chemical transport models.

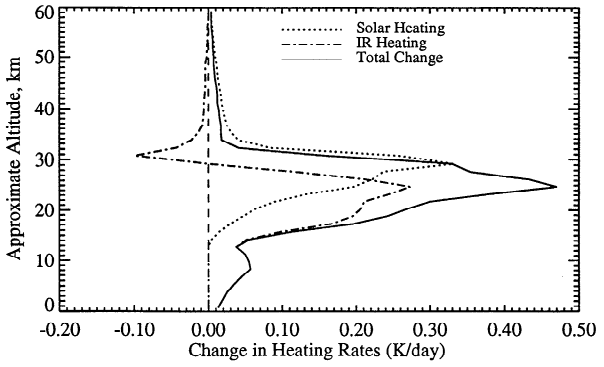

Figure 5. The change in solar, infrared, and total heating due to aerosol from Mount Pinatubo near the equator during mid-October 1991.

We found the chemical effects of changes in the radiation field were almost entirely attributable to changes in aerosol heating rates; the changes due to direct photolysis effects were insignificant. The net effect of photolysis decreased ozone in October/November 1991 by less than 1 DU (see Table 1, case D). Increasing the aerosol extinction will affect the amount of UV visible flux in the lower stratosphere. *Pitari and Rizi* [1993] derived large changes in the molecular oxygen photodissociation rate (J_{O_2}), which affected the ozone production rate in the lower stratosphere. This caused a sizable decrease in both local (−8%) and column ozone (−5%) ozone. We get a similar overall shape for the change in J_{O_2} in this study, compared to theirs, except our J_{O_2} change occurs approximately 5 km lower in the stratosphere. They show a J_{O_2} decrease of 5% at 25 km increasing to about 20% at 20 km. We derive a 0% decrease in J_{O_2} at 25 km and a 5% decrease at 20 km. Since our change in J_{O_2} peaks below the ozone maximum, we see little effect on column ozone. That *Pitari and Rizi* [1993] found photolysis effects to be much more important is almost certainly explained by the much larger wavelength dependence they used for UV visible aerosol extinctions.

In summary, considering only the effects on temperature

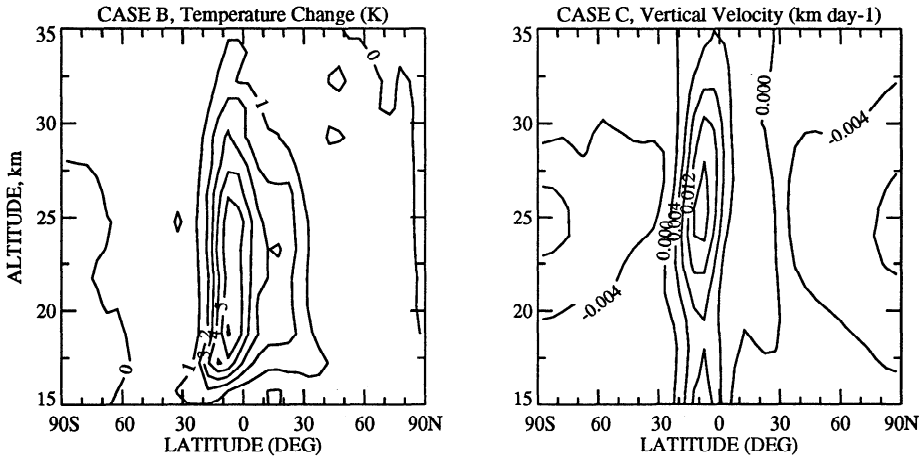

Figure 6. Model-derived effect of increased optical extinction on local temperature or vertical wind velocity for October 15, 1991. (left) Model-derived temperature change (in Kelvins) for case B. (right) Model-derived change in vertical winds for case C. In either case, all of the net heating for Mount Pinatubo aerosols was channeled into either a temperature or dynamical perturbation.

and circulation from Mount Pinatubo aerosol induced change in heating rates, the LLNL 2-D results suggest that in late 1991 the observed change in ozone is in better agreement when the change in heating rate is channeled into increasing the mean circulation strength. When the change in heating rate following the eruption is completely channeled into temperature change, the resulting effect on reaction rates that modify odd-oxygen loss would underestimate the observed change. The observed increase in ozone above 28 km as described by *Grant et al.* [1994] and *Hofmann et al.* [1994] is not represented in the model cases (B and C). Comparison of the total vertical rise is slightly less than what *DeMore et al.* [1992] would suggest. This study does not show the large decrease in local and column ozone derived by *Pitari and Rizi* [1993] when Mount Pinatubo induced changes in photolysis are considered. It is difficult to envision a scenario, even in a completely coupled model, where both the change in ozone from increased circulation and the change in stratospheric temperatures could simultaneously be derived that compare adequately with observed data. For example, in the case of *Brasseur and Granier* [1992], which is a fully interactive model calculation, they under-

Table 3. Change in Equatorial 1991 Column Ozone (Dobson Units) Following the Mount Pinatubo Eruptions

	July	Aug.	Sept.	Oct.	Nov.	Dec.
			Previous Studies			
TOMS satellite	+5	−2	−8	−14	−18	
Ozonesondes (16–28 km)		−23 ± 6	−29 ± 9	−25 ± 6	−25 ± 6	−8 ± 6
Ozonesondes (28–31 km)		+4.6 ± 2	+5.9 ± 2	+3.1 ± 2	+2.0 ± 2	+4.6 ± 2
Model [*Kinne et al.*, 1992]	−7	−17	−22	−26	−26	
			LLNL 2-D Model Study			
Case B (MtP ext, bkg SAD) temp allowed to change	−0.2	−1.1	−2.8	−3.9	−4.9	−5.0
Case C (MtP ext, bkg SAD) PSI allowed to change	−1.0	−6.8	−14	−17	−16	−12
Case D (MtP ext, bkg SAD) PSI and temp are fixed	−0.02	−0.05	−0.14	−0.38	−0.71	−0.87
Case E (bkg ext, MtP SAD) PSI and temp are fixed	−1.2	−2.5	−2.9	−3.8	−4.6	−5.0
Case F (bkg ext, 2 × MtP SAD) PSI and temp are fixed	−1.5	−3.3	−4.1	−5.2	−5.9	−6.2
Case G (MtP ext, MtP SAD) temp allowed to change	−1.5	−3.7	−6.2	−8.1	−9.4	−9.6
Case H (MtP ext, MtP SAD) PSI allowed to change	−2.2	−8.7	−16	−19	−19	−16

Values for total ozone mapping spectrometer (TOMS) are taken from *Schoeberl et al.* [1993] (listed by *Kinne et al.* [1992, Table 8]). Ozonesondes partial-column data are taken from *Grant et al.* [1994]. *Grant et al.* [1994] relates the change from electrochemical concentrations cell (ECC) sonde data relative to stratospheric aerosol and gas experiment II (SAGE II) climatology between 16–28 km and 28–31 km.

Abbreviations for the LLNL study are bkg ext, background optical extinction is included; MtP ext, Mount Pinatubo optical extinction is included; bkg SAD, background surface area density is included; MtP SAD, Mount Pinatubo surface area density is included; PSI, seasonally varying circulation stream function; and temp, seasonally varying temperature distribution.

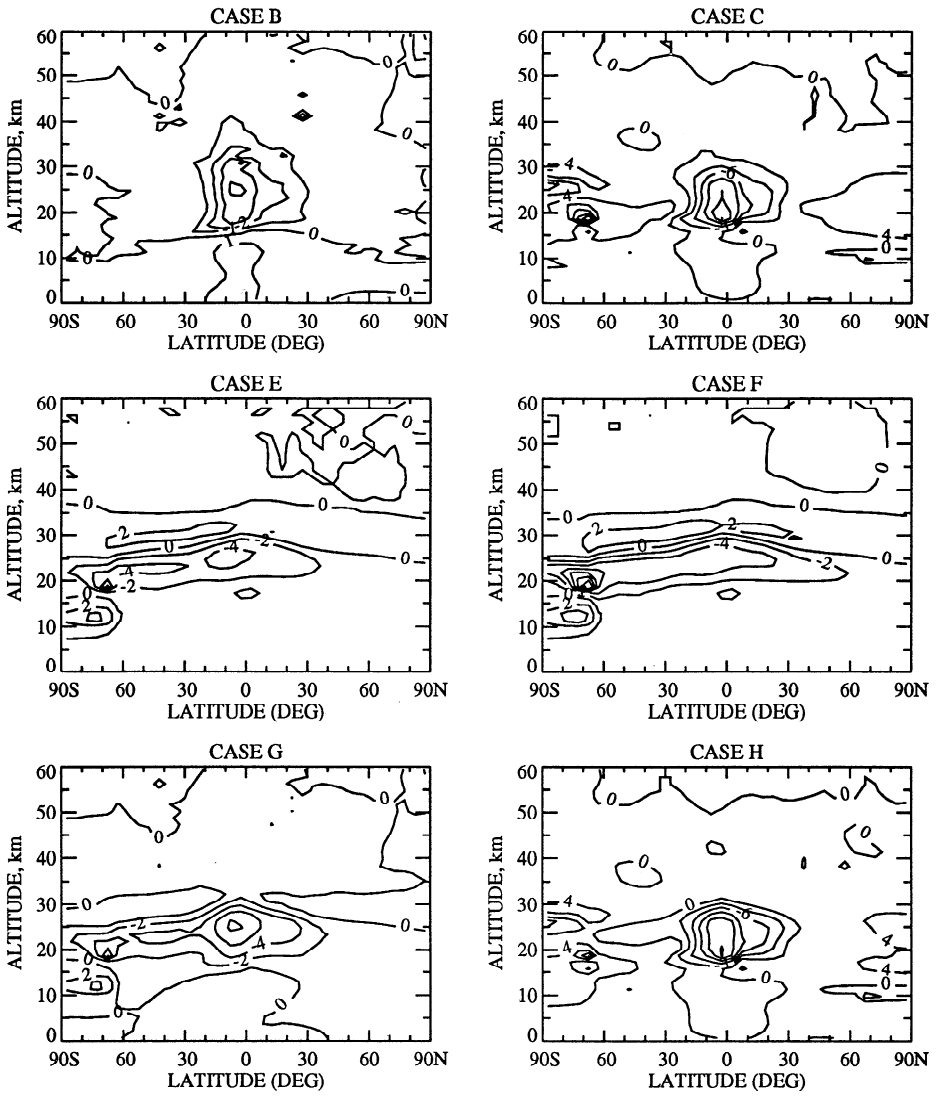

Figure 7. Model-derived percentage change in ozone for cases B, C, E, F, G, and H on October 15, 1991 (see Table 1).

estimate the adiabatic rising contribution and overestimate the temperature change compared to observed data. In addition, their local ozone change is substantially less than that measured by *Grant et al.* [1994] or inferred from TOMS column data. Changes in model-derived column ozone in 1992 and 1993 in general are not represented correctly when only aerosol heating effects are considered. In the next section, the potential effect of heterogeneous chemical processes on sulfate aerosols is discussed. In this section the seasonally varying circulation and the temperature distributions are held fixed to ambient nonvolcanic conditions.

Including Heterogeneous Reactions on Sulfate Aerosols

Time-dependent aerosol surface area density data (SAD) for the post Mount Pinatubo period were also derived from the SAGE II retrievals (L. Thomason, NASA Langley Research Center, private communication, 1993; also see *Thomason* [1991] for data retrieval procedure). Sixteen different swaths were used between June 1991 and November 1993. After November 1993 a 1-year decay time constant was assumed for the rest of 1993. For swaths that were saturated, the same procedure of applying lidar data discussed in the radiative effects section is used here. For high latitudes where SAGE II data are not measured, the SAD is quadratically extrapolated to the pole. In Figure 10, examples of several swaths are shown for the background SAD (ambient) up through the swath of April 10 to May 20, 1993. The maximum SAD derived by Thomason from the SAGE II data peaked approximately during the December 1991/ January 1992 period. In order to investigate the effect of uncertainties in the derived SAD, we created a scenario where the time-dependent SAD was multiplied by a factor of 2 (Table 1, case F).

Nonvolcanic atmosphere. In assessing the effect of increased surface area density following the Mount Pinatubo eruption, it is first important to understand the odd-oxygen loss controlling process in the ambient nonvolcanic atmosphere (case A). The catalytic cycles believed to be the most important in the lower stratosphere are the following:

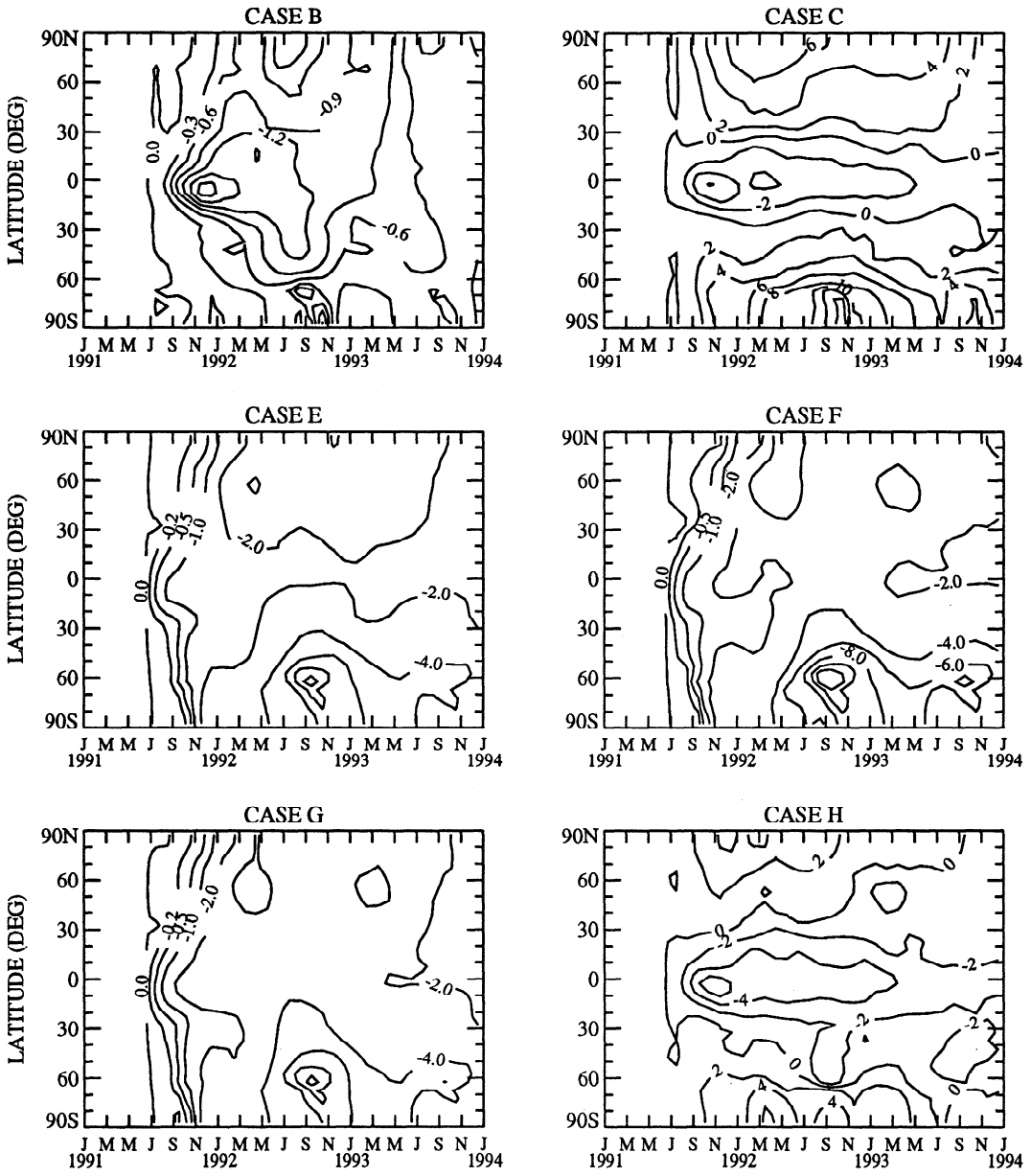

Figure 8. Time-dependent model-derived percentage change in total ozone for cases B, C, E, F, G, and H.

Cycle 1

$$NO + O_3 \rightarrow NO_2 + O_2$$
$$NO_2 + O \rightarrow NO + O_2$$
$$O_3 + O \rightarrow 2O_2$$

Cycle 2

$$OH + O_3 \rightarrow HO_2 + O_2$$
$$HO_2 + O_3 \rightarrow OH + 2O_2$$
$$O_3 + O \rightarrow 2O_2$$

Cycle 3

$$Cl + O_3 \rightarrow ClO + O_2$$
$$ClO + O \rightarrow Cl + O_2$$
$$O_3 + O \rightarrow 2O_2$$

Cycle 4

$$OH + O_3 \rightarrow HO_2 + O_2$$
$$Cl + O_3 \rightarrow ClO + O_2$$
$$HO_2 + ClO \rightarrow HOCl + O_2$$
$$HOCl + h\nu \rightarrow Cl + OH$$
$$O_3 + O_3 \rightarrow 3O_2$$

Cycle 5

$$Cl + O_3 \rightarrow ClO + O_2$$
$$Br + O_3 \rightarrow BrO + O_2$$
$$ClO + BrO \rightarrow Br + ClOO$$
$$ClOO + M \rightarrow Cl + O_2 + M$$
$$O_3 + O_3 \rightarrow 3O_2$$

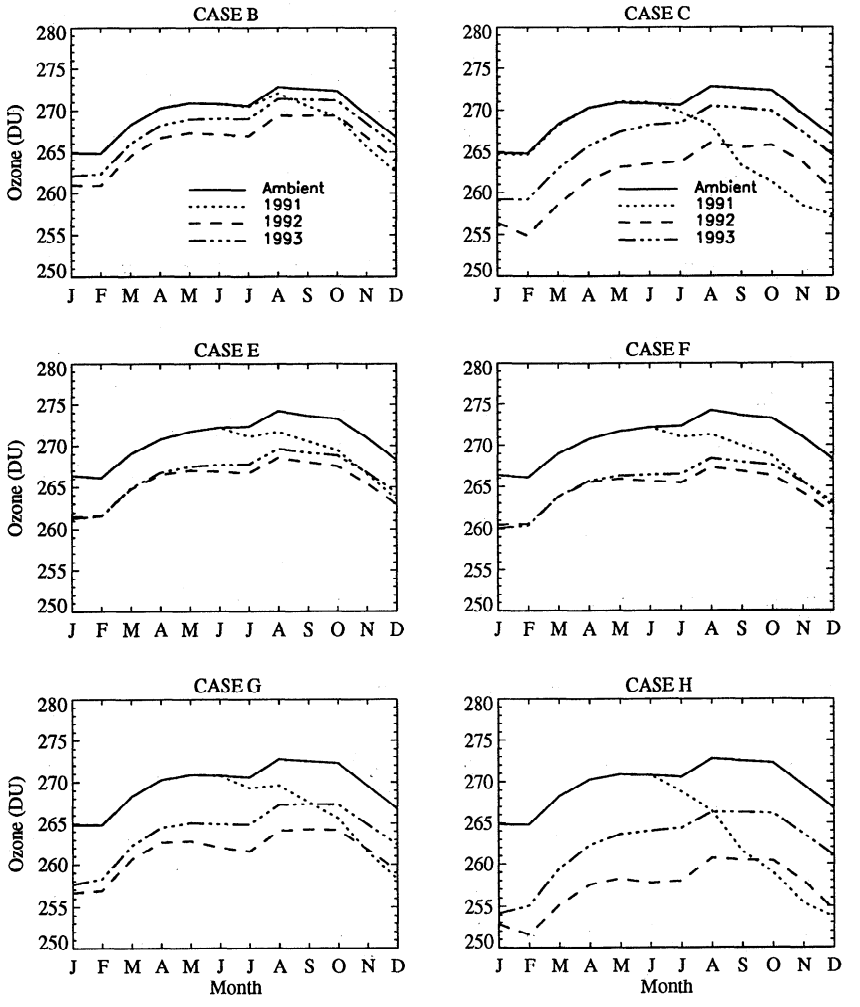

Figure 9. Seasonal variability in total ozone (Dobson units) averaged between 12.5°S and 12.5°N for the ambient (case A) and cases B, C, E, F, G, and H during 1991, 1992, and 1993.

Cycle 6

$$Cl + O_3 \rightarrow ClO + O_2$$
$$Br + O_3 \rightarrow BrO + O_2$$
$$ClO + BrO \rightarrow BrCl + O_2$$
$$BrCl + h\nu \rightarrow Br + Cl$$
$$\overline{O_3 + O_3 \rightarrow 3O_2}$$

Cycle 7

$$Cl + O_3 \rightarrow ClO + O_2$$
$$Cl + O_3 \rightarrow ClO + O_2$$
$$ClO + ClO + M \rightarrow Cl_2O_2 + M$$
$$Cl_2O_2 + h\nu \rightarrow Cl + ClOO$$
$$ClOO + M \rightarrow Cl + O_2 + M$$
$$\overline{O_3 + O_3 \rightarrow 3O_2}$$

For a chemical reaction mechanism that includes only gas phase reactions (not included in the tables or figures), cycle 1 is the most important odd-oxygen loss process in the lower stratosphere. When the heterogeneous reactions (6) and (7)

Table 4. Model-Derived Percent Change in Column Ozone

Case (Year)	Region					
	Global	NH	SH	65°S–65°N	12°S–12°N	30°N–60°N
B(1991)	−0.17	−0.16	−0.19	−0.20	−0.43	−0.07
B(1992)	−0.96	−0.97	−0.94	−1.02	−1.27	−0.82
B(1993)	−0.59	−0.64	−0.54	−0.60	−0.63	−0.66
C(1991)	0.10	0.19	0.02	−0.06	−1.44	0.77
C(1992)	1.39	1.26	1.53	0.61	−2.83	3.36
C(1993)	1.02	1.26	0.75	0.58	−1.26	2.23
E(1991)	−0.40	−0.33	−0.48	−0.42	−0.61	−0.23
E(1992)	−2.78	−2.33	−3.26	−2.67	−1.90	−2.73
E(1993)	−2.41	−2.06	−2.79	−2.31	−1.63	−2.41
F(1991)	−0.52	−0.39	−0.66	−0.54	−0.73	−0.27
F(1992)	−3.55	−2.95	−4.19	−3.40	−2.32	−3.49
F(1993)	−3.18	−2.63	−3.77	−3.04	−2.07	−3.10
G(1991)	−0.57	−0.49	−0.66	−0.61	−1.01	−0.31
G(1992)	−3.53	−3.15	−3.94	−3.50	−3.01	−3.37
G(1993)	−2.74	−2.49	−3.01	−2.66	−2.09	−2.82
H(1991)	−0.25	−0.13	−0.39	−0.42	−1.84	0.49
H(1992)	−1.55	−1.35	−1.76	−2.12	−4.61	0.15
H(1993)	−1.49	−1.28	−1.72	−1.73	−2.71	−0.98

NH is northern hemisphere, and SH is southern hemisphere.

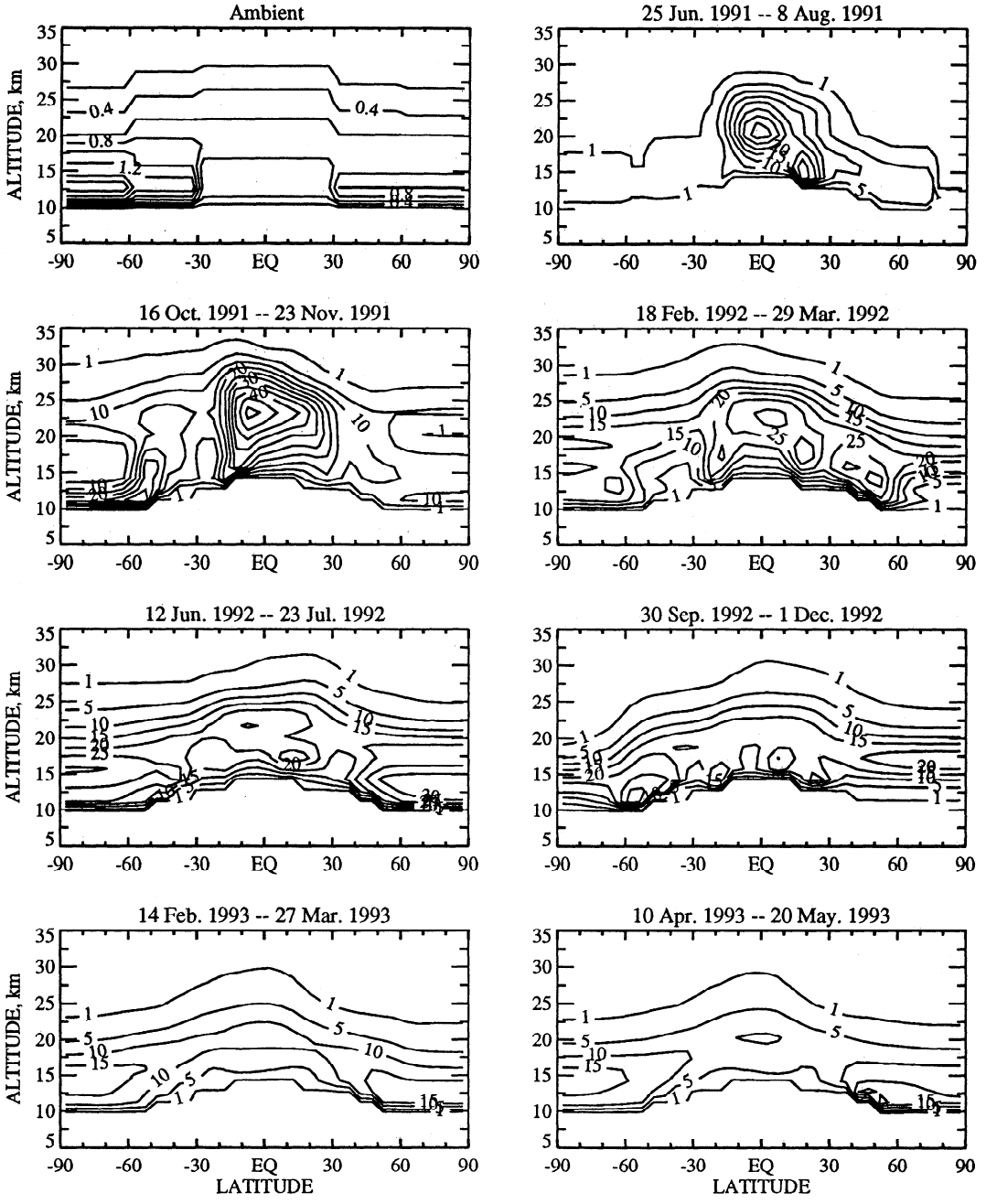

Figure 10. Surface area density (in square microns per cubic centimeter) derived from the Stratospheric Aerosol and Gas Experiment II (SAGE II) satellite for background and times following the Mount Pinatubo eruption.

are included in the chemical mechanism for the reference atmosphere, the odd-oxygen loss from catalytic cycles 2–7 increase in relative importance to cycle 1 (NO_2 + O). For example, in the equatorial region, at 23 km, (Table 5) the major odd-oxygen loss process is from cycle 2 (HO_2 + O_3), accounting for 41% of the total odd-oxygen loss. Cycle 1 is the second most important process, followed by cycle 3 (ClO + O) and cycle 4 (HOCl + $h\nu$). Cycles 5 and 6 (ClO + BrO), which include species from both the BrO_x and ClO_x chemical families, account for 4.6% of the total odd-oxygen loss in the equatorial region. For midlatitude, northern hemisphere winter, at 23 km, cycle 2 (HO_2 + O_3) is 27% of the total odd-oxygen loss for the reference atmosphere, followed by cycle 1 (NO_2 + O) and cycle 2 (ClO + O) at 21% and 20%, respectively. During winter at high latitudes, cycle 5 (ClO + BrO) becomes more important because it is not as dependent on photolysis to complete the cycle. For the midlatitude southern hemisphere during this period (summer), the major odd-oxygen loss process in the lower stratosphere is cycle 1 (NO_2 + O), followed by cycle 2 (HO_2 + O_3) and cycle 3 (ClO + O). This seasonal difference for cycle 1 (NO_2 + O) is based on the abundance of NO and NO_2 during the winter season. With decreases in ultraviolet solar flux at high latitudes in the winter hemisphere, more NO_x is converted to N_2O_5 and eventually converted to HNO_3 by reaction (6). Because of the strong coupling between chemical families,

Table 5. Odd-Oxygen Loss for the Most Important Catalytic Cycles in the Lower Stratosphere (23 km) on December 15, 1991

Catalytic Cycle Rate Limiting Reaction	Loss at 42.5°S, %		Loss at Equator, %		Loss at 42.5°N, %	
	Reference Atmosphere	With Pinatubo	Reference Atmosphere	With Pinatubo	Reference Atmosphere	With Pinatubo
$O_3 + O$	9.8	8.2	7.7	5.7	12.6	7.9
$HO_2 + O_3$	22.5	27.5	40.8	38.4	26.5	21.1
$HO_2 + O$	2.2	2.6	3.5	3.3	1.7	1.4
$NO_2 + O$	42.0	24.3	19.5	10.4	21.2	6.6
$ClO + O$	12.4	18.0	12.4	16.1	20.2	28.7
$Cl_2O_2 + h\nu$	0.3	0.7	0.4	0.9	0.8	2.6
$HOCl + h\nu$	5.9	11.7	10.0	16.5	6.8	12.7
$ClO + BrO$	3.1	6.3	4.6	7.4	8.7	17.7
$BrO + BrO$	0.1	0.1	0.1	0.2	0.2	0.3
$BrO + O$	0.6	0.8	0.9	0.8	1.2	1.0
Odd Oxygen Loss Rate, molecules cm^{-3} s^{-1}	263,000	272,000	93,200	123,000	83,000	128,000

The reference atmosphere is case A, and the Mount Pinatubo atmosphere is case E.

and with the decrease of ambient NO_x concentrations and of ClO_x, HO_x, and BrO_x concentrations, the rates of cycles 2–7 increase relative to cycle 1.

Atmosphere perturbed by Mount Pinatubo. Ignoring the effect of aerosol heating and scattering from the increased Mount Pinatubo optical extinction, but allowing the SAD to vary with time, increasing the rates of (6) and (7) does modify the partitioning of odd-oxygen loss between chemical families. Including Mount Pinatubo SAD, cycle 1 (NO_2 + O), in the equatorial region, lower stratosphere, is now a minor odd-oxygen loss process (approximately 10% of the total). HO_x is still the major odd-oxygen loss family; cycle 2 ($HO_2 + O_3$) accounts for 38% of the total odd-oxygen loss. Cycle 4 ($HOCl + h\nu$) and the sum of cycles 5 and 6 (ClO + BrO) increase by 65% and 61%, respectively, relative to the reference atmosphere. At midlatitudes, cycle 3 ($ClO + O$) is the major odd-oxygen loss process. Cycle 2 ($HO_2 + O_3$) and the sum of cycles 5 and 6 (ClO + BrO) are next, followed by cycle 4 ($HOCl + h\nu$). Cycle 1 ($NO_2 + O$) accounts for only 7% of the total. At latitudes greater than 42.5°N the ClO + BrO catalytic cycles are the dominant odd-oxygen loss processes in the lower stratosphere. Model-derived total odd-oxygen loss in the lower stratosphere equatorial and midlatitude regions increased by 32% and 54%, respectively. In the southern hemisphere, total odd-oxygen loss increases by 3% relative to the reference atmosphere; however, the absolute change in molecules per cubic centimeter per second is still sizable.

Prather [1992] used a photochemical model to investigate the potential catastrophic loss of stratospheric ozone from increased SAD following a volcanic eruption. He varied the SAD from less than background up to approximately 1000 times background. In his study, rapid ozone loss begins to occur when the noontime NO_x mixing ratio falls below 600 pptv, and Antarctic-like losses occur when noontime NO_x decreases to 200 pptv. In this study, using time-dependent SAGE II derived SAD (Figure 3), the SAD does not increase to a large enough value to cause catastrophic ozone loss. Even if the SAGE II time-dependent SAD is arbitrarily multiplied by 2 (Figure 11), ozone concentrations do not show a large additional decrease (compare cases E and F, Figures 7 and 8). The effect on reaction (6) from the change in SAD is shown in Figure 11. With SAGE II SAD the rate of this reaction increases dramatically in both the equatorial and midlatitude regions. When the SAGE II SAD is multiplied by 2, in both the equator and midlatitude southern hemisphere, the rate of $N_2O_5 + H_2O$ between 15 km and 26 km and between 15 km and 24 km, respectively, did not change. Above these altitude ranges, doubling the SAD increased the rate by between 30% and 40%. *Brasseur and Granier* [1992], *Pitari and Rizi* [1993], and *Rodriguez et al.* [1994] also notice a similar behavior in their model studies.

There is a large seasonal variation in the $N_2O_5 + H_2O$ rate. Figure 12 shows the rate of $N_2O_5 + H_2O$ at two months (July and December) and two latitudes (equator and 42°S). Here the largest increase from the Mount Pinatubo eruption on the rate of (6) is in the summer hemisphere where the maximum diurnal-averaged reaction precursors to N_2O_5 formation, NO_2 and NO_3, are maximized. This can also be seen in the magnitude of the ambient atmosphere N_2O_5 (Table 6) mixing ratio, where, in mid-December lower stratosphere, the mixing ratio is 316, 92, and 213 pptv for 42.5°S, equator, and 42.5°N, respectively. After the eruption the rate for this reaction remains saturated in the lower stratosphere through December 15, 1993, for all latitudes and times. In the middle stratosphere the largest change in Figure 12 is in the summer hemisphere at 42°S, where the maximum rate increases by over a factor of 3 by December 15, 1991. At 20 km, by December 15, 1993, the rate is a factor of 2 greater than the ambient. In the winter hemisphere the additional SAD from Mount Pinatubo did not dramatically change $N_2O_5 + H_2O$ rate from July 1991 through July 1993 relative to the ambient case. In the equatorial region, model-derived changes in the rate of this reaction were enhanced throughout 1991, 1992, and 1993 relative to the ambient case. The enhancement of this rate is still over a factor of 2 greater in December 1993. After examining the time series, it is evident that the model-derived $N_2O_5 + H_2O$ rate is still sizable 1.5 years after the June 15 eruption.

For reaction (7) ($ClONO_2 + H_2O$) the effect of changing the SAD is quite different. Unlike (6), this reaction does not saturate in the lower stratosphere. In fact, when the SAD was doubled, the rate of this reaction increased approximately linearly (Figure 13) at both the equator and 63°S. The seasonal dependence of this reaction is shown in both Figures 13 and 14. Here the months of April, September, and

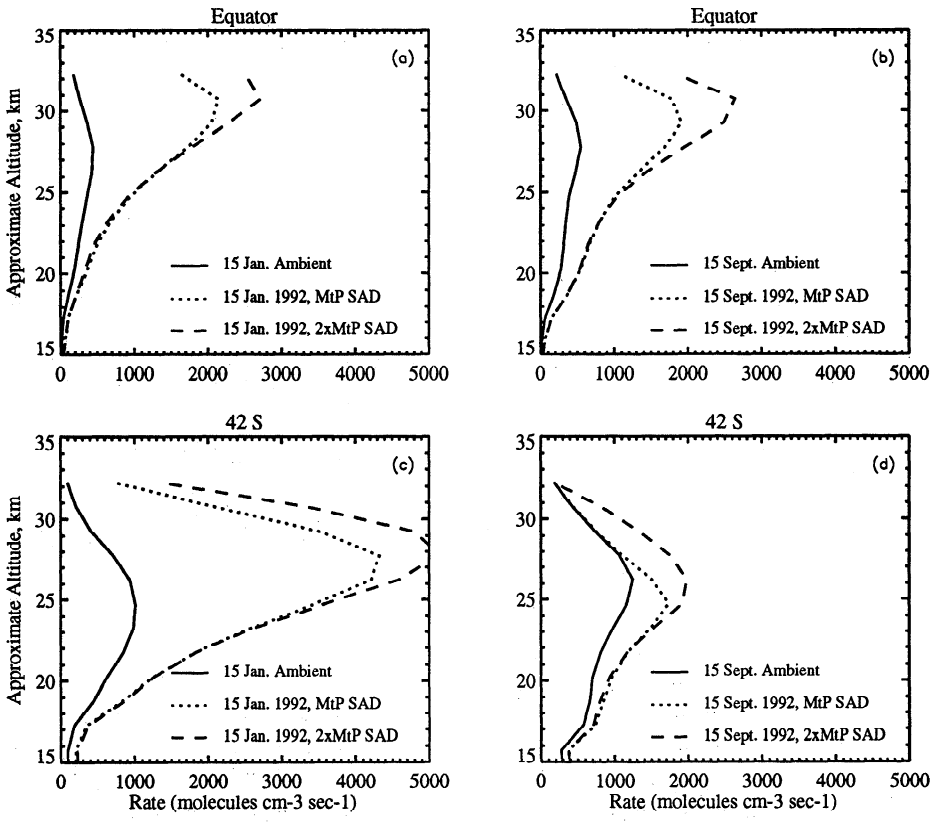

Figure 11. Rate of reaction of $N_2O_5 + H_2O \rightarrow 2HNO_3$ (in molecules per cubic centimeter per second) on the surface of sulfate aerosols at the equator and 42°S. Both January and September periods are considered for both the ambient (case A) and the 1992 Mount Pinatubo perturbed (cases E and F (2 × surface area density (SAD) of Mount Pinatubo)) atmospheres.

January are highlighted. Since this reaction increases with decreasing temperature (or decreasing H_2SO_4 wt %), September, which has the coldest temperature, shows the largest increase in rate (note the scale change in both Figures 13 and 14). *Prather* [1992] suggests that (7) is primarily the mechanism for suppressing NO_x below values produced by (6). As shown in Figure 13, (7) is not near saturation under Mount Pinatubo conditions. A much larger eruption, as modeled by *Prather* [1992], would cause greater decreases in ozone from sulfate aerosol heterogeneous chemistry. The time-dependent variation of (7) at the equator and 63°S for April and September is shown in Figure 14. Notice that the equatorial rate is approximately a factor of 10 less than the rate at 63°S in September. In the equatorial region the rate in September 1991 is about twice as large as that for September 1992 and 4 times that for September 1993. At higher latitudes the increased SAD from Mount Pinatubo is still relatively small in September of 1991. Therefore the peak rate in Figure 14 occurs in September of 1992. It is interesting to compare the rate of (7) in April 1992 to September 1992. Because of the temperature dependence of this rate the impact on chemical partitioning and odd-oxygen loss is much greater during the colder temperature in September.

In Table 6 the diurnally averaged mixing ratios for NO_x, ClO_x, HO_x, BrO_x, HOCl, HCl, $ClONO_2$, HNO_3, and N_2O_5, and also the NO_2/NO, ClO/Cl, and HO_2/OH ratios in the lower stratosphere (23 km) are listed (same conditions as Table 5). It is evident that at the latitudes listed in Table 6, the model-derived N_2O_5 concentration has been significantly decreased relative to the nonvolcanic value, consistent with the increased rates for (6) and (7) discussed above. In fact, the equatorial N_2O_5 mixing ratio has decreased by 95%. Under the same conditions, NO_x has decreased by 38%. Comparing the change in the mixing ratio of these two species from the eruption suggests that the formation step $NO_2 + NO_3$ is the rate-limiting step for conversion of NO_x to HNO_3 via (6). Concurrently, both ClO_x and HO_x have increased. As described by *Granier and Brasseur* [1992], the conversion of NO_x to HNO_3 via sulfate heterogeneous reactions changes the partitioning and increases HO_x from the decreased rate of $NO_2 + OH + M \rightarrow HNO_3 + M$ (Table 7), based on lower NO_2 concentration driven by (6) and (7). As HO_x increases, the reaction of $HCl + OH \rightarrow Cl + H_2O$ increases ClO_x. In this study, the HCl concentration decreased (Table 6) primarily from this reaction and because the formation reaction $Cl + CH_4 \rightarrow HCl$ is not as fast (Table 7). Another interesting effect of lower NO_x is the change in partitioning between ClO and Cl. As NO decreases, the $ClO + NO \rightarrow NO_2 + Cl$ rate decreases, increasing the ratio of ClO/Cl. With more HO_x and ClO_x, and the reactions of ClO_x with BrO_x, more odd-oxygen is destroyed when the SAD is increased. In addition, model-derived $ClONO_2$ concentration increased slightly following the eruption. Since the level of ClO_x increased and since ClO_x is the limiting reactant, the net effect is a slight increase in $ClONO_2$ (see Tables 6 and 7). This will change as the rate of (7) increases above a critical level as discussed by *Prather* [1992].

The NO_2 column at Lauder, New Zealand (45°S, 170°E),

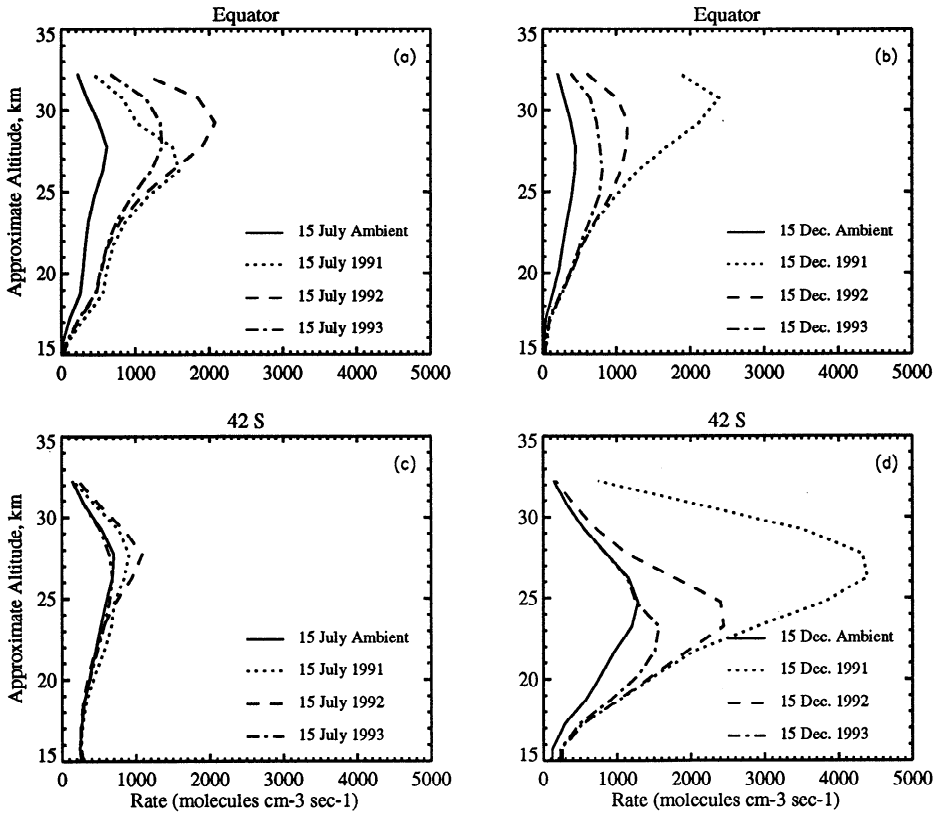

Figure 12. Rate of reaction of $N_2O_5 + H_2O \rightarrow 2HNO_3$ (in molecules per cubic centimeter per second) on the surface of sulfate aerosols at the equator and 42°S. Both July and December periods in 1991, 1992, and 1993 are considered for both the ambient (case A) and the Mount Pinatubo perturbed (case E) model-derived atmospheres.

has been measured over the last 11 years. During the period after the Mount Pinatubo eruption, data collected at 45°S had anomalously low values of slant column NO_2 [*Johnston et al.*, 1992]. NO_2 column data were observed to decrease by as much as 40%, peaking in October 1991. Model-derived column NO_2 decrease (not shown) peaked at −12% at 42.5°S in October 1991. The period of the peak change in NO_2 derived by the model is consistent with observed data. The apparent discrepancy in the observed versus model-derived magnitude of the change in column NO_2 may be partially explained by the increased uncertainty in the observations. Changes in the aerosol scattering can change the measure-

Table 6. Species Diurnal-Averaged Mixing Ratio Values in the Lower Stratosphere (23 km) on December 15, 1991

	42.5°S		Equator		42.5°N	
Species	Reference Atmosphere	With Pinatubo	Reference Atmosphere	With Pinatubo	Reference Atmosphere	With Pinatubo
NO_x	1580	978	592	367	372	190
ClO_x	45.9	75.5	25.3	41.4	35.9	71.9
HO_x	4.80	6.41	4.03	4.90	1.60	1.96
BrO_x	3.48	4.52	2.68	3.26	2.66	3.65
HOCl	15.6	34.5	14.6	30.0	24.4	60.4
HCl	1420	1350	800	775	1240	1140
$ClONO_2$	1040	1060	310	312	762	781
HNO_3	7420	8600	2700	3110	9160	9820
N_2O_5	316	28.6	91.8	4.08	213	8.50
O_3	3.57	3.35	2.88	2.76	4.00	3.82
NO_2/NO	2.98	3.07	2.84	3.02	5.60	6.33
ClO/Cl	1910	2890	2970	4430	8090	15200
HO_2/OH	6.24	7.33	6.98	7.87	10.7	10.3

Units for all species are in parts per trillion by volume except O_3 which is in parts per million by volume. The reference atmosphere is case A, and the Mount Pinatubo atmosphere is case E. NO_x = $NO + NO_2$; ClO_x = Cl + ClO; HO_x = OH + HO_2; and BrO_x = Br + BrO.

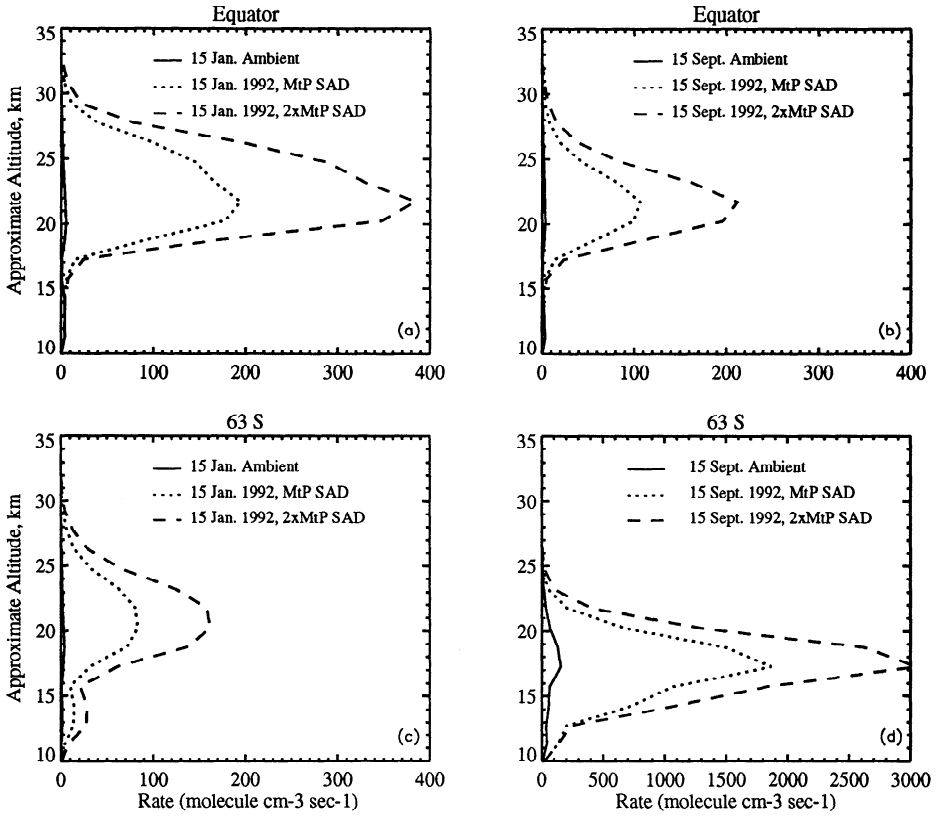

Figure 13. Rate of reaction of $ClONO_2 + H_2O \rightarrow HOCl + HNO_3$ (in molecules per cubic centimeter per second) on the surface of sulfate aerosols at the equator and 63°S. Both January and September periods are considered for both the ambient (case A) and the 1992 Mount Pinatubo perturbed (cases E and F (2 × surface area density (SAD) of Mount Pinatubo)) atmospheres.

ment geometry. However, even when this is taken into account, the minimum change in slant column NO_2 is estimated to be greater than −20%. Adding the heterogeneous reactions (6) and (7) does improve the agreement of HNO_3 in the reference atmosphere to observed data taken by the limb infrared monitor of the stratosphere (LIMS) on the Nimbus 7 satellite (not shown). However, reference model-derived NO_2 does not compare well to NO_2 data collected by LIMS [*Considine et al.*, 1992; *Granier and Brasseur*, 1992]. In general, model-derived NO_2 is lower than observed data at middle to high latitudes in the lower stratosphere. Therefore the model-derived reference atmosphere (without any volcanic perturbation) is not currently representing the NO_2-controlling chemical processes accurately. This may adversely affect the sensitivity in calculated column NO_2 with respect to *Johnston et al.* [1992]. A detailed analysis of both the observed column NO_2 and HNO_3 compared to the LLNL and AER 2-D models is presented by *Koike et al.* [1994].

The time-dependent model-derived local (25 km) changes in NO_x, ClO_x, and HO_x are shown in Figure 15 for cases E and H at both equatorial latitudes and 42.5°S (similar to Lauder, New Zealand). Here for case E, heterogeneous effects only, there is a rapid change following the June 15 eruption at both the equator and 42.5°S. At 42.5°S the effect of the seasonal variation in the mean circulation can be seen. The local change in NO_x is consistent with the column change measured at Lauder, New Zealand (mentioned above). This would suggest that the model-derived column NO_2 is peaking at a higher altitude, possibly from dynamical discrepancies. Notice that by December 1994, model-derived NO_x in the equatorial region is still 25% below ambient concentrations. This is not true at higher latitudes, where the aerosol distribution has settled to a lower altitude, and local processing of NO_x is small. In fact, at 42.5°S and 20 km altitude, NO_x concentration is 20% below ambient value (not shown), similar to equatorial conditions at 25 km. Similar arguments can be made for ClO_x and HO_x. The effect of heterogeneous forcing plus the circulation forcing induced by excess volcanic aerosol (case H) will be discussed in the next section.

Local (Figure 7) and column (Figures 8, 9, and 16; Tables 3 and 4) ozone changes for case E (SAGE II derived SAD) and case F (2 times SAGE II SAD) are very different than case C (aerosol heating modifying circulation). In 1991 the model-derived equatorial change in Dobson units for cases E and F (Table 3) underestimates the observed change from TOMS and ozonesonde data. Even when the time-dependent SAD is multiplied by 2, the additional ozone loss is still too small. The maximum equatorial change for case E is approximately −2% in late 1991 through 1993 (Figure 8). Local equatorial changes in October 1991 are between −4% and −5% between 20 and 25 km (Figure 7). The recovery time for change in equatorial ozone is much slower for case E relative to case C. In fact, the model-derived equatorial change in ozone is as large in December of 1993 as it was in December of 1991 (Figure 9). In contrast, when circulation feedback for aerosol heating is considered (case C), the equatorial ozone

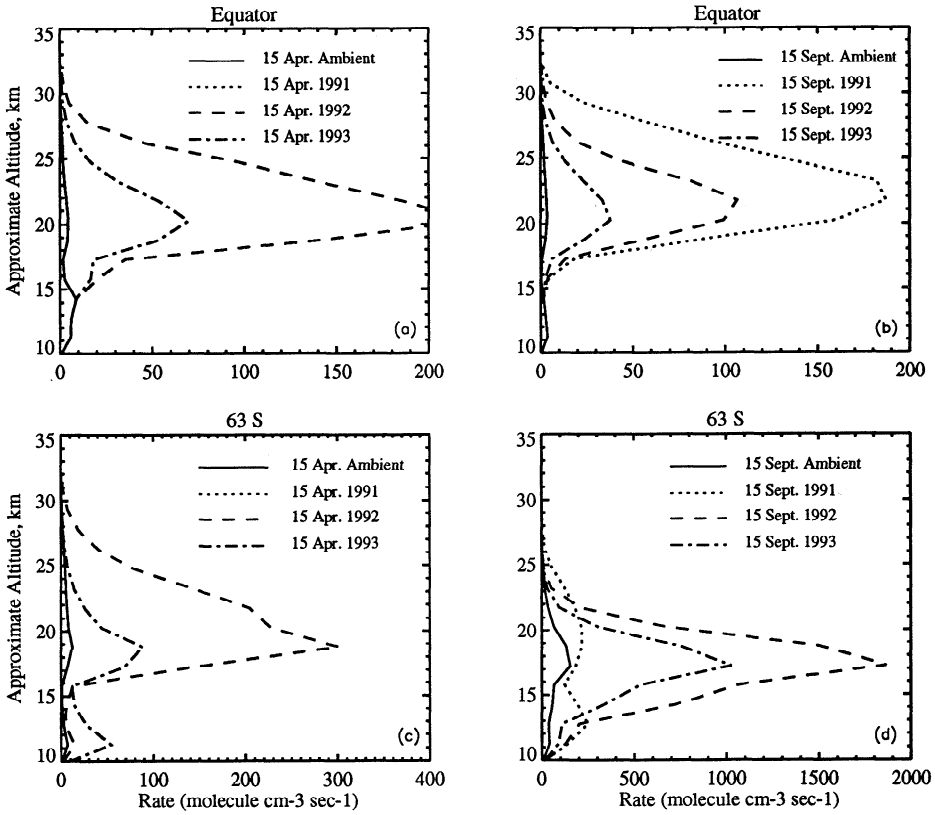

Figure 14. Rate of reaction of $ClONO_2 + H_2O \rightarrow HOCl + HNO_3$ (in molecules per cubic centimeter per second) on the surface of sulfate aerosols at the equator and 63°S. Both July and December periods in 1991, 1992, and 1993 are considered for both the ambient (case A) and the Mount Pinatubo perturbed (case E) model-derived atmospheres.

approaches nonvolcanic values by December 1993. Model-derived column changes are larger in the midlatitude region than in the equatorial region. For case E the 30°N–60°N region shows a −2.7% and −2.4% decrease in 1992 and 1993, respectively (Table 4). At 12°S–12°N the change in column ozone is −1.9% and −1.6% in 1992 and 1993, respectively. This is consistent with the TOMS studies of both *Gleason et al.* [1993] and *Herman and Larko* [1994], which both show larger change in column ozone at middle to high latitudes relative to the equatorial region. The model, however, does not derive the large 1993 column ozone changes described by *Herman and Larko* [1994] at middle to high latitudes in the northern hemisphere. Comparing Figure 9 (equatorial) and Figure 16 (midlatitude), the contrast of circulation feedback and heterogeneous chemistry on column ozone is quite different within these regions. At midlatitudes, column ozone, case C, increases after the eruption through December 1993 (Figure 16). Under the same condition, case E is less than the ambient through 1993. The model also does not show a higher decrease in column ozone in the NH compared to the SH as the measurements suggest. The model-derived 65°S–65°N column ozone decrease (−2.3%) is comparable to the observed change (−3%) between 70°S and 70°N [*Herman and Larko*, 1994]. Other time-dependent modeling studies, for example, that of *Pitari and Rizi* [1993], show considerably higher ozone depletion from heterogeneous processing on sulfate aerosols. They derived in April of 1992, for 60°N, a −12% column ozone change. *Rodriguez et al.* [1994] under similar conditions, derived −3% column ozone change, similar to this study. It is possible that *Pitari*

Table 7. Reaction Rates in the Lower Stratosphere (23 km) on December 15, 1991

Reaction Rate, molecules cm^{-3} s^{-1}	42.5°S		Equator		42.5°N	
	Reference Atmosphere	With Pinatubo	Reference Atmosphere	With Pinatubo	Reference Atmosphere	With Pinatubo
$ClO + NO_2$	4.59 (4)	4.72 (4)	1.08 (4)	1.11 (4)	1.34 (4)	1.55 (4)
$ClO + NO$	1.24 (6)	1.24 (6)	3.79 (5)	3.68 (5)	2.46 (5)	2.28 (5)
$Cl + CH_4$	808	882	370	392	174	186
$OH + HCl$	868	957	379	404	157	184
$OH + NO_2$	5860	4240	1750	1210	421	279

The reference atmosphere is case A, and the Mount Pinatubo atmosphere is case E. Read 4.59 (4) as 4.59×10^4.

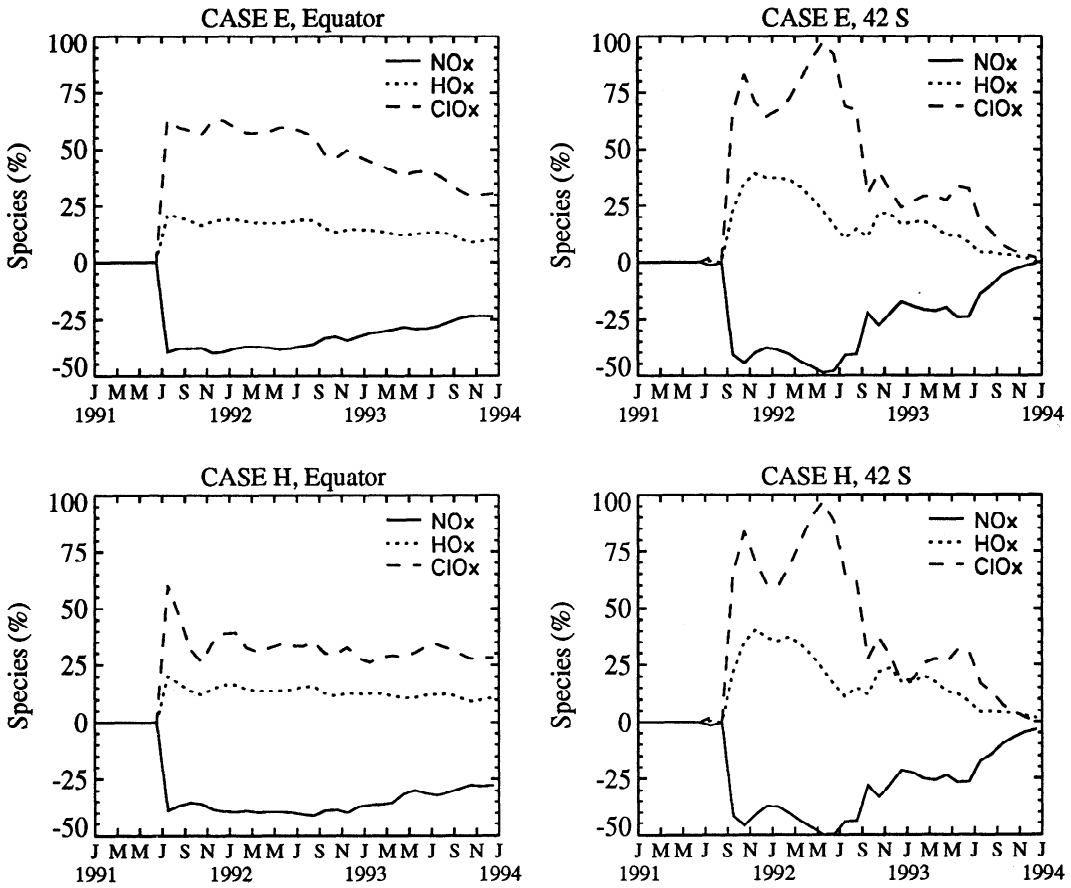

Figure 15. Time-dependent percentage change in local (25 km) NO_x (NO + NO_2), ClO_x (Cl + ClO), and HO_x (OH + HO_2) for cases E and H at the equator and 42°S.

and Rizi [1993] have colder model temperatures and therefore derive much larger processing rates via (7) than those calculated in this study or by *Rodriguez et al.* [1994]. High-latitude polar ozone decreases, above what is normally derived from PSC related heterogeneous chemical processes, are also represented in this study (Figure 8). For case E a −10% ozone reduction is derived, peaking in the southern hemisphere in September/October 1992. A similar change, but lower in magnitude (−4%), is derived in the northern hemisphere during the 1992 April/May period. The same latitude and period change in column ozone is derived in 1993, but with lower absolute decreases. The polar processes represented in this version of the LLNL 2-D CRT are adequate to represent the gross features of the high-latitude heterogeneous processes, but detailed model/data comparisons are not appropriate and are left for future 3-D studies.

In summary, model-derived ozone change from heterogeneous reactions on sulfate aerosols can significantly reduce column ozone following an eruption the size of Mount Pinatubo. Including both (6) and (7) with the inclusion of time-dependent SAD produces model-derived reductions in column ozone following the eruption in 1991. These reactions may help explain a portion of the observed change during this period. There is a sizable change in midlatitude column ozone relative to the equatorial region, which is consistent in latitude but not magnitude with observed data. The large observed change in equatorial ozone during late 1991 cannot be explained using (6) and (7). In the next section, both the heterogeneous and the aerosol heating impact on ozone are examined.

Combined Radiative and Chemical Effects

The effects of combining the chemical and radiative effects, either on temperature or circulation, on the change in ozone can be seen in Figure 8. Here, the combined features in cases G (heterogeneous plus aerosol heating, allowing temperature to vary) and case H (heterogeneous plus aerosol heating, allowing circulation to be modified) can be compared to the individual processes that occur following a volcanic eruption. In case G the individual effects of aerosol heating, modifying temperature, and the heterogeneous processes on sulfate aerosols when combined are approximately additive with respect to the individual effects. For example, in Table 3 the change in equatorial ozone in Dobson units for October 15, 1991, is −3.9, −3.8, and −8.1 for cases B, E, and G, respectively. A similar statement can be made for case H. Here for the same region and period the change in Dobson units is −17, −3.8, and −19 for cases C, E, and H, respectively. Case G underestimates the observed equatorial ozone change in October 1991 by approximately 40% compared to TOMS [*Schoeberl et al.*, 1993] and sizably more compared to the ozonesonde data of *Grant et al.* [1994]. However, case G compared to TOMS slightly overestimates the change in Dobson units between July and September

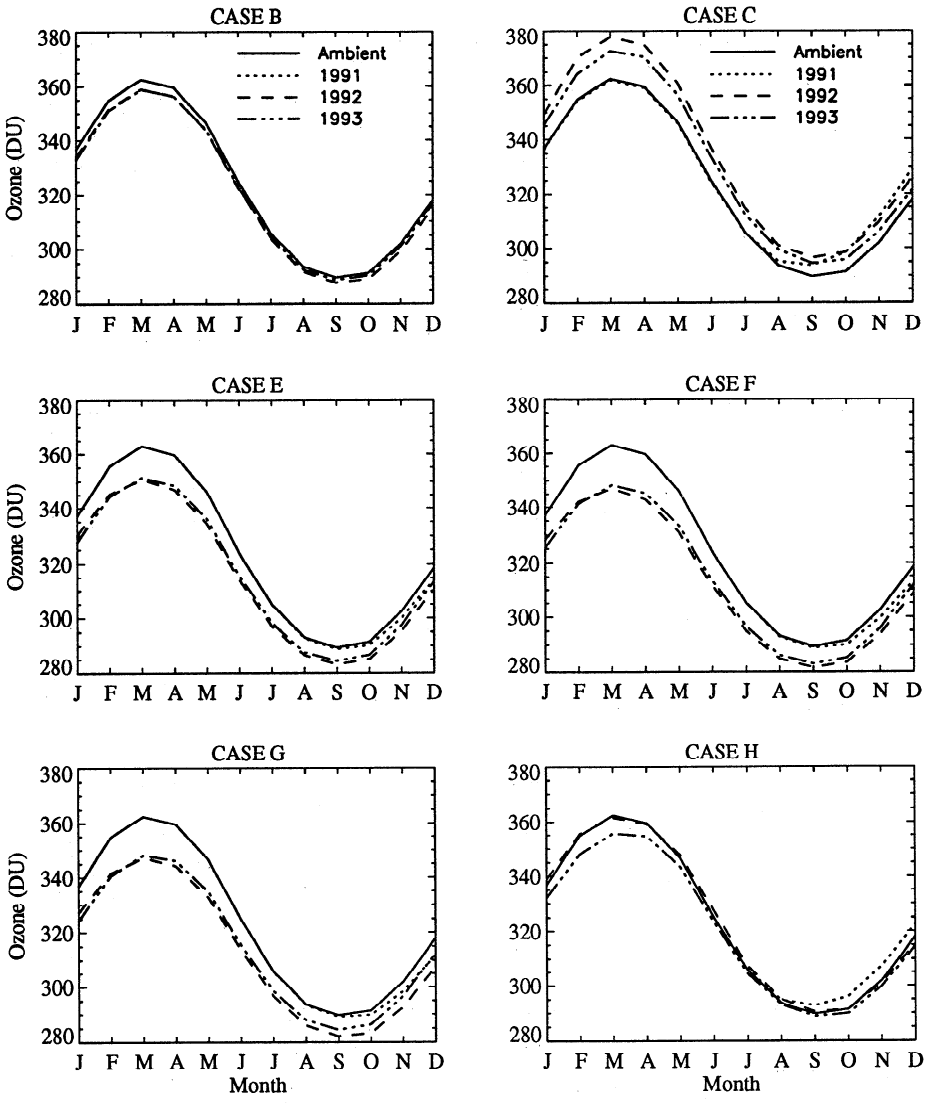

Figure 16. Seasonal variability in total ozone (Dobson units) averaged between 30°N and 60°N for the ambient (case A) and cases B, C, E, F, G, and H during 1991, 1992, and 1993.

1991. The opposite is true when comparing to *Grant et al.* [1994]. The peak in equatorial ozone change for case G is not consistent with either TOMS or the ozonesonde data (Table 3 and Figure 8). For case H, model-derived ozone compares moderately with TOMS in peak magnitude and period. Case H overestimates the reduction between July and September 1991 and is on the lower end of the peak magnitude range compared to the ozonesonde data. Model-derived local equatorial ozone changes (Figure 7) show reductions of −8% and −12% in the lower stratosphere for cases G and H, respectively. These changes even for case H are sizably less than that derived from *Grant et al.* [1994]. In general, case H better represents the 1991 observed equatorial ozone data. At extratropical latitudes, when case H is considered, there is a cancellation of the positive ozone production from an increased mean circulation and a decrease from increased heterogeneous processing. In Table 4 the net annual affect on ozone from case H at midlatitudes (30°N–60°N) is +0.5%, +0.2%, and −1% for 1991, 1992, and 1993, respectively. Additional changes in NO_x, HO_x, and ClO_x also can be seen when circulation feedback is included (Figure 15). Here comparisons of case H and case E at the equator and 42°S (close to Lauder, New Zealand) show slightly different changes in these species when circulation feedback is included. The effect is more pronounced in the equatorial region.

In summary, if the 2-D model dynamical approach is reasonable and there is production of ozone at higher latitudes from increased circulation, then the model-derived heterogeneous effects must be considerably larger to explain the observed data; alternatively, the dynamical processes not included in the LLNL 2-D model (e.g., QBO) are responsible for a large portion of the 1992 and 1993 ozone reductions.

Conclusions

We have represented the Mount Pinatubo eruption in a detailed manner allowing us to compare directly to observed temperature and species distributions and their changes from the eruption through 1993. In the model approach used here, combined effects of heterogeneous chemistry and circulation

change are necessary to explain observed measurements. We do not believe that this result is sensitive to the uncertainties in the aerosol distribution and its time evolution. Vertical lofting was approximately consistent with observation as was the ozone change in the equatorial region. In a zonally average diabatic approach, a consequence of strengthened mean circulation is transport of ozone toward the pole. This produces a positive global ozone change that does not agree with TOMS, unless the change is mitigated by including heterogeneously driven chemical ozone loss. However, even with an observationally based aerosol distribution, differences are evident between the model results and observations. The model predicts ozone increases at middle and high latitudes that appear not to be observed. Complete understanding of the partitioning of aerosol heating into both temperature and circulation along with a true understanding of volcanically induced heterogeneous effects at high latitude polar winter conditions will need to be addressed in a 3-D model.

The net heating rate forcing derived from the mid-October equatorial extinction data is 0.48 K/day (25 km) of which 0.28 is from IR heating and 0.2 is from solar heating (Figure 5). The solar heating is directly related to the choice of single-scattering albedo, which in this study was 0.99 throughout all cases. The IR heating rate is solely dependent on the observed data and the LLNL IR submodel. The IR heating in this study is consistent with that of *Kinne et al.* [1992]; however, the solar heating is larger.

When circulation alone (case C) was allowed to vary with fixed seasonally varying temperatures, large local (−10%) and column (−6%) equatorial ozone changes were derived in October/November of 1991 (Tables 3 and 4; Figures 7–9). The vertical velocity was enhanced, displacing the ozone column by approximately 1.6 km in 100 days (Figure 6). These equatorial column ozone reductions are generally consistent with observed data of TOMS [*Schoeberl et al.*, 1993]. The model-derived results underestimate the ozone magnitude relative to the ozonesonde data derived by *Grant et al.* [1994]. The model-derived equatorial maximum decrease was in October 1991, peaking slightly before TOMS. The model-derived ozone decrease was much less than shown by the ozonesonde data in August 1991. The strengthening of the mean circulation not only caused local ozone depletion in the equatorial region but also enhanced local ozone amounts in the mid- to high-latitude regions (Figures 8 and 16). Global change in column ozone for 1991, 1992, and 1993 was 0.1, 1.4, and 1.0, respectively. Equatorial (12°S–12°N) column ozone change for 1991, 1992, and 1993 was −1.4, −2.8, and −1.3, respectively, in better agreement with observed TOMS and ozonesonde data. In general, case C reproduces the observed data only in the equatorial region; the ozone production at high latitudes is not evident in the observed data and may be a limitation in the dynamical assumptions and sophistication of a zonally averaged 2-D model.

Allowing the temperature to change but holding the circulation seasonally fixed (case B) modified the lower stratospheric temperature by +2 K for 20°N and by +5 to +6 K in the equatorial region (Figure 6). This is in good agreement with *Labitzke and McCormick* [1992] at 20°N, but it overestimates the equatorial value by up to 2 K. Equatorial ozone change from this case underestimated the local and column amounts relative to observed measurements. Equatorial local and column ozone changes between August and December 1991 did not represent the observed data. Global change in column ozone for 1991, 1992, and 1993 is −0.2, −1.0, and −0.6, respectively, which also is an underestimate of the TOMS observed data. Extratropical latitude reductions in ozone did occur in 1991–1993, but they not as large as reported by TOMS [*Herman and Larko*, 1994].

With the circulation and temperature fields held seasonally fixed but the Mount Pinatubo aerosol extinction allowed to change the direct and indirect flux, the photolysis coefficients were slightly modified (case D). We found this effect to be a minor perturbation to the ozone distribution in the stratosphere (Table 3). This is in disagreement with *Pitari and Rizi* [1993], who found a significant ozone perturbation from this effect. They had a larger extinction at UV wavelengths affecting photolysis. Validation of the SAGE II profiles in general confirm a relatively flat wavelength dependence.

Including the effect of SAGE II time-dependent SAD only on modifying heterogeneous reaction rates, keeping both temperature and circulation seasonally fixed (case E), increased the hydrolysis of N_2O_5 and $ClONO_2$ significantly. As a sensitivity test, the time-dependent SAD was doubled (case F; Figures 11 and 13). For N_2O_5 hydrolysis the reaction saturated in the equatorial region between 15 and 26 km and between 15 and 24 km at 42°S throughout 1991, 1992, and 1993 (Figure 12). For $ClONO_2$ hydrolysis the equatorial rates were much less than the high-latitude rates, and under the SAD studies (cases E and F) modeled here, saturation of this reaction was not observed. Changes in odd-oxygen loss were derived (Table 5). After Mount Pinatubo the HO_x family is the primary loss process for odd-oxygen in the lower stratosphere, followed by ClO_x and NO_x (Table 5). Changes in model-derived species concentrations (Table 6 and Figure 15) are sizable, for example, at 23 km, 43°N, on December 15, 1991: NO_x (−50%), followed by increases in ClO_x (100%) and HO_x (23%). NO_x is decreased by direct conversion of N_2O_5 and $ClONO_2$ on sulfate aerosols. HO_x is increased from this reduction in NO_x, forming less HNO_3 via reaction with OH. HCl is decreased primary from reaction with enhanced OH, releasing more ClO_x. $ClONO_2$ increases slightly from increases in enhanced ClO_x (Table 7). Decreases in column NO_2 and increases in column HNO_3 are consistent with the Lauder, New Zealand, data [*Johnston et al.*, 1992], peaking in October 1991. The magnitude of the column NO_2 change is less than observed. Changes in equatorial local (4%) and column (1.5%) ozone were not large enough to explain the observed data in 1991 (Tables 3 and 4; Figures 7–9). Overall, the heterogeneous effect on ozone in 1991 was 25% of the circulation effect (case C). Changes in 1992 and 1993 show extratropical reductions that are consistent in latitude, but TOMS and ground-based data are still underestimated (Tables 3 and 4; Figures 7–9 and 16).

Including both aerosol extinction modification of either temperature or circulation with the enhanced heterogeneous processing on sulfate aerosols improves model/data comparison of local and column ozone in various regions and times. For example, in 1991, equatorial ozone amounts compare better to the observed data when aerosol-modified circulation and enhanced heterogeneous processing (case H) are combined (Tables 3 and 4; Figures 7–9). At extratropical latitudes the increase from the circulation feedback and the

decrease in ozone from heterogeneous processing tend to cancel, and, as a consequence, the agreement with observed data is not as good. When temperature is allowed to vary, with a fixed seasonally varying circulation plus the heterogeneous effect (case G), the midlatitude change in ozone is more spatially representative of the 1992 and 1993 TOMS data; however, the model-derived maximum ozone reduction is not large enough.

In summary, using the LLNL 2-D CRT model, we investigated the individual contributions from chemistry, radiative transfer, and dynamics following a major volcanic eruption focusing on the relative importance of circulation versus temperature change. Model-derived changes in species distribution and temperature were compared to observed data. This study is the groundwork for future studies that will use both a fully interactive 2-D model and a 3-D model. Validating the model-derived absolute change in trace species and the response time for change in these concentrations following a documented volcanic eruption like Mount Pinatubo will build confidence in our current understanding of stratospheric processes and the use of these models for prognostic purposes.

Acknowledgments. The authors wish to thank Larry Thomason (NASA Langley Research Center) and John Mergenthaler (Lockheed Palo Alto Research Labs) for helpful discussions relating to SAGE II and CLAES data, respectively. SAGE II data were obtained from and with the help of the user support offices of the NASA/GSFC and NASA/Langley Distributed Active Archive Centers. CLAES data were obtained from the UARS Central Data Handling Facility. Terry Deshler (University of Wyoming) provided lidar profiles used for patching saturated SAGE II profiles. We are additionally grateful to Larry Thomason for supplying us with the SAGE II derived surface area densities used in this study. Tom Kuczmarski (LLNL) provided essential data analysis and graphics support. In addition, we would like to thank the reviewers of this article for their diligence and useful comments. The research was partially funded by the UARS program and was supported in part by the NASA Atmospheric Chemistry Modeling and Analysis Program and the Department of Energy's Office of Health and Environmental Research, Environmental Science Division. It was performed under the auspices of the U.S. Department of Energy by the Lawrence Livermore National Laboratory under contract W-7405-Eng-48.

References

Alaka, M., and R. C. Elvander, Optimum interpolation from observations of mixed quality, *Mon. Weather Rev.*, *100*, 612–624, 1972.

Bekki, S., R. Toumi, and J. A. Pyle, Role of sulfur photochemistry in tropical ozone changes after the eruption of Mount Pinatubo, *Nature*, *362*, 331–333, 1993.

Beyerle, G., R. Neuber, O. Schrems, F. Wittrock, and B. Knudsen, Multiwavelength lidar measurements of stratospheric aerosols above Spitsbergen during winter 1992/93, *Geophys. Res. Lett.*, *21*, 57–60, 1994.

Bluth, G. J. S., S. D. Doiron, C. C. Schnetzler, A. J. Krueger, and L. S. Walter, Global tracking of the SO_2 clouds from the June 1991 Mount Pinatubo eruptions, *Geophys. Res. Lett.*, *19*, 151–154, 1992.

Bojkov, R. D., C. S. Zerefos, D. S. Balis, I. C. Ziomas, and A. F. Bais, Record low total ozone during northern winters of 1992 and 1993, *Geophys. Res. Lett.*, *20*, 1351–1354, 1993.

Boville, B. A., J. R. Holton, and P. W. Mote, Simulation of the Pinatubo aerosol cloud in general circulation model, *Geophys. Res. Lett.*, *18*, 2281–2284, 1991.

Brasseur, G. P., and C. Granier, Mount Pinatubo aerosols, chlorofluorocarbons, and ozone depletion, *Science*, *257*, 1239–1242, 1992.

Brasseur, G. P., C. Granier, and S. Walters, Future change in stratospheric ozone and the role of heterogeneous chemistry, *Nature*, *348*, 626–628, 1990.

Burley, J. D., and H. S. Johnston, Ionic mechanisms for heterogeneous stratospheric reactions and ultraviolet photoabsorption cross sections for NO_2^+, HNO_3, and NO_3^- in sulfuric acid, *Geophys. Res. Lett.*, *19*, 1359–1366, 1992a.

Burley, J. D., and H. S. Johnston, Nitrosyl sulfuric acid and stratospheric aerosols, *Geophys. Res. Lett.*, *19*, 1363–1366, 1992b.

Chandra, S., Changes in stratospheric ozone and temperature after the eruption of Mount Pinatubo, *Geophys. Res. Lett.*, *20*, 33–36, 1993.

Considine, D. B., A. R. Douglass, and R. S. Stolarski, Heterogeneous conversion of N_2O_5 to HNO_3 on background stratospheric aerosols: Comparisons of model results with data, *Geophys. Res. Lett.*, *19*, 397–400, 1992.

DeFoor, T. E., E. Robinson, and S. Ryan, Early lidar observations of the June 1991 Pinatubo eruption plume at Mauna Loa Observatory, Hawaii, *Geophys. Res. Lett.*, *19*, 187–190, 1992.

DeLuisi, J. J., E. G. Dutton, K. L. Coulson, T. E. DeFoor, and B. G. Mendonca, On some radiative features of the El Chichon volcanic stratospheric dust cloud and a cloud of unknown origin observed at Mauna Loa, *J. Geophys. Res.*, *88*, 6769–6772, 1983.

DeMore, W. B., S. P. Sander, D. M. Golden, M. J. Molina, R. F. Hampson, M. J. Kurylo, C. J. Howard, A. R. Ravishankara, and C. E. Kolb, Chemical kinetics and photochemical data for use in stratospheric modeling, Evaluation Number 10, *JPL Publ.*, *92-20*, Aug. 15, 1992.

Deshler, T., A. Adriani, G. P. Gobbi, D. J. Hofmann, G. Di Donfrancesco, and B. J. Johnson, Volcanic aerosol and ozone depletion within the antarctic polar vortex during the austral spring of 1991, *Geophys. Res. Lett.*, *19*, 1819–1822, 1992a.

Deshler, T., D. J. Hofmann, B. J. Johnson, and W. R. Rozier, Balloonborne measurements of the Pinatubo aerosol size distribution and volatility at Laramie, Wyoming during the summer of 1991, *Geophys. Res. Lett.*, *19*, 199–202, 1992b.

Deshler, T., B. J. Johnson, and W. R. Rozier, Balloonborne measurements of Pinatubo aerosol during 1991 and 1992 at 41°N: Vertical profiles, size distribution, and volatility, *Geophys. Res. Lett.*, *20*, 1435–1438, 1993.

Fahey, D. W., et al., In situ measurements constraining the role of sulfate aerosols in mid-latitude ozone depletion, *Nature*, *363*, 509–514, 1993.

Froidevaux, L., J. W. Waters, W. G. Read, L. S. Elson, D. A. Flower, and R. F. Jarnot, Global ozone from UARS MLS: An overview of zonal mean results, *J. Atmos. Sci.*, in press, 1994.

Gleason, J. F., et al., Record low global ozone in 1992, *Science*, *260*, 523–526, 1993.

Granger, R. G., A. Lambert, F. W. Taylor, J. J. Remedios, C. D. Rogers, M. Corney, and B. J. Kerridge, Infrared absorption by volcanic stratospheric aerosols observed by ISAMS, *Geophys. Res. Lett.*, *20*, 1283–1286, 1993.

Granier, C., and G. Brasseur, Impact of heterogeneous chemistry on model predictions of ozone change, *J. Geophys. Res.*, *97*, 18,015–18,033, 1992.

Grant, W. B., et al., Observations of reduced ozone concentrations in the tropical stratosphere after the eruption of Mount Pinatubo, *Geophys. Res. Lett.*, *19*, 1109–1112, 1992.

Grant, W. B., et al., Aerosol-associated changes in tropical stratospheric ozone following the eruption of Mount Pinatubo, *J. Geophys. Res.*, *99*, 8197–8211, 1994.

Hanson, D. R., and A. R. Ravishankara, The reaction probabilities of $ClONO_2$ and N_2O_5 on 40 to 75% sulfuric acid solutions, *J. Geophys. Res.*, *96*, 17,307–17,314, 1991.

Hanson, D. R., and A. R. Ravishankara, Reaction of $ClONO_2$ with HCl on NAT, NAD, and frozen sulfuric acid and hydrolysis of N_2O_5 and $ClONO_2$ on frozen sulfuric acid, *J. Geophys. Res.*, *98*, 22,931–22,936, 1993.

Hanson, D. R., A. R. Ravishankara, and S. Solomon, Heterogeneous reactions in sulfuric acid aerosols: A framework for model calculations, *J. Geophys. Res.*, *99*, 3615–3629, 1994.

Herman, J. R., and D. Larko, Low ozone amounts during 1992–1993 from Nimbus 7 and Meteor 3 total ozone mapping spectrometers, *J. Geophys. Res.*, *99*, 3483–3496, 1994.

Hofmann, D. J., and S. J. Oltmans, Anomalous Antarctic ozone

during 1992: Evidence for Pinatubo volcanic aerosol effects, *J. Geophys. Res.*, *98*, 18,555–18,561, 1993.

Hofmann, D. J., and J. M. Rosen, Sulfuric acid droplet formation and growth in the stratosphere after the 1982 eruption of El Chichón, *Science*, *222*, 325–327, 1983.

Hofmann, D. J., and S. Solomon, Ozone destruction through heterogeneous chemistry following the eruption of El Chichon, *J. Geophys. Res.*, *94*, 5029–5041, 1989.

Hofmann, D. J., S. J. Oltmans, J. M. Harris, S. Solomon, T. Deshler, and B. J. Johnson, Observation and possible causes of new ozone depletion in Antarctica in 1991, *Nature*, *359*, 283–287, 1992.

Hofmann, D. J., S. J. Oltmans, W. D. Komhyr, J. M. Harris, J. A. Lathrop, A. O. Langford, T. Deshler, B. J. Johnson, A. Torres, and W. A. Matthews, *Geophys. Res. Lett.*, *21*, 65–68, 1994.

Johnston, P. V., R. L. Mckenzie, J. G. Keys, and W. A. Matthews, Observations of depleted stratospheric NO_2 following the Pinatubo volcanic eruption, *Geophys. Res. Lett.*, *19*, 211–213, 1992.

Journel, A. G., *Fundamentals of Geostatistics in Five Lessons*, *Short Course*, vol. 8, AGU, Washington, D. C., 1989.

Kerr, J. B., D. I. Wardle, and D. W. Tarasick, Record low ozone values over Canada in early 1993, *Geophys. Res. Lett.*, *20*, 1979–1982, 1993.

Kinne, S., O. B. Toon, and M. J. Prather, Buffering of stratospheric circulation by changing amounts of tropical ozone: A Pinatubo case study, *Geophys. Res. Lett.*, *19*, 1927–1930, 1992.

Kinnison, D. E., K. E. Grant, P. S. Connell, and D. J. Wuebbles, Effects of the Mount Pinatubo eruption on the radiative and chemical processes in the troposphere and stratosphere, in *International Quadrennial Ozone Symposium*, edited by R. D. Hudson, June 4–13, 1992.

Koike, M., N. B. Jones, W. A. Matthews, P. V. Johnston, R. L. McKenzie, D. E. Kinnison, and J. Rodriguez, Impact of Pinatubo aerosols on the partitioning between NO_2 and HNO_3, *Geophys. Res. Lett.*, *21*, 597–600, 1994.

Komhyr, W. D., R. D. Grass, R. D. Evans, R. K. Leonard, and D. M. Quincy, Unprecedented 1993 ozone decrease over the United States from Dobson spectrophotometer observations, *Geophys. Res. Lett.*, *21*, 201–204, 1994.

Labitzke, K., and M. P. McCormick, Stratospheric temperature increases due to Pinatubo aerosols, *Geophys. Res. Lett.*, *19*, 207–210, 1992.

McCormick, M. P., and R. E. Veiga, SAGE II measurements of early Pinatubo aerosols, *Geophys. Res. Lett.*, *19*, 155–158, 1992.

Mergenthaler, J. L., J. B. Kumer, and A. E. Roche, CLAES south-looking aerosol observations for 1992, *Geophys. Res. Lett.*, *20*, 1295–1298, 1993.

Michelangeli, D. V., M. Allen, and Y. L. Yung, El Chichon volcanic aerosols: Impact of radiative, thermal, and chemical perturbations, *J. Geophys. Res.*, *94*, 18,429–18,443, 1989.

Molina, M. J., R. Zhang, P. J. Wooldridge, J. R. McMahon, J. E. Kim, H. Y. Chang, and D. Beyer, Physical chemistry of the $H_2SO_4/HNO_3/H_2O$ system: Implications for polar stratospheric clouds, *Science*, *261*, 1418–1423, 1993.

Mozurkewich, M., and J. G. Calvert, Reaction probability of N_2O_5 on aqueous aerosols, *J. Geophys. Res.*, *93*, 15,889–15,896, 1988.

Ogren, J. A., N. C. Ahlquist, A. D. Clarke, and R. J. Charlson, Measurements of the absorption coefficient of stratospheric aerosols, *Geophys. Res. Lett.*, *8*, 9–12, 1981.

Patten, K. O., Jr., P. S. Connell, D. E. Kinnison, D. J. Wuebbles, T. G. Slanger, and L. Froidevaux, Effect of vibrationally excited oxygen on ozone production in the stratosphere, *J. Geophys. Res.*, *99*, 1211–1224, 1994.

Peixoto, J. P., and A. H. Oort, *Physics of Climate*, American Institute of Physics, New York, 1992.

Pitari, G., A numerical study of the possible perturbation of stratospheric dynamics due to Pinatubo aerosols: Implications for tracer transport, *J. Atmos. Sci.*, *50*, 2443–2461, 1993.

Pitari, G., and V. Rizi, An estimate of the chemical and radiative perturbation of stratospheric ozone following the eruption of Mount Pinatubo, *J. Atmos. Sci.*, *50*, 3260–3276, 1993.

Prather, M., Catastrophic loss of stratospheric ozone in dense volcanic clouds, *J. Geophys. Res.*, *97*, 10,187–10,191, 1992.

Prather, M. J., H. L. Wesoky, R. C. Miake-Lye, A. R. Douglass, R. P. Turco, D. J. Wuebbles, M. K. W. Ko, and A. L. Schmeltekopf, The atmospheric effects of stratospheric aircraft: A first program report, *NASA Ref. Publ. 1272*, 1992.

Pueschel, R. F., D. F. Blake, K. G. Snetsinger, A. D. A. Hansen, S. Verma, and K. Kato, Black carbon (soot) aerosol in the lower stratosphere and upper troposphere, *Geophys. Res. Lett.*, *19*, 1659–1662, 1992.

Rodgers, C. D., Retrieval of atmospheric temperature and composition from remote measurements of thermal radiation, *Rev. Geophys.*, *14*, 609–624, 1976.

Rodriguez, J. M., M. K. W. Ko, and N. D. Sze, Role of heterogeneous conversion of N_2O_5 on sulfate aerosols in global ozone losses, *Nature*, *352*, 134–137, 1991.

Rodriguez, J. M., M. K. W. Ko, N. D. Sze, C. E. Heisey, G. K. Yue, and M. P. McCormick, Ozone response to enhanced heterogeneous processing after the eruption of Mount Pinatubo, *Geophys. Res. Lett.*, *21*, 209–212, 1994.

Russell, P. B., and M. P. McCormick, SAGE II aerosol data validation and initial data use: An introduction and overview, *J. Geophys. Res.*, *94*, 8335–8338, 1989.

Russell, P. B., et al., Post-Pinatubo optical depth spectra vs. latitude and vortex structure: Airborne tracking sunphotometer measurements in AASE II, *Geophys. Res. Lett.*, *20*, 2571–2574, 1993a.

Russell, P. B., et al., Pinatubo and pre-Pinatubo optical-depth spectra: Mauna Loa measurements, comparisons, inferred particle size distributions, radiative effects, and relationship to lidar data, *J. Geophys. Res.*, *98*, 22,969–22,985, 1993b.

Schoeberl, M. R., P. K. Bhartia, and E. Hilsenrath, Tropical ozone loss following the eruption of Mount Pinatubo, *Geophys. Res. Lett.*, *20*, 29–32, 1993.

Solomon, S., R. W. Sanders, R. R. Garcia, and J. G. Keys, Increased chlorine dioxide over Antarctica caused by volcanic aerosols from Mount Pinatubo, *Nature*, *363*, 245–248, 1993.

Solomon, S., R. W. Sanders, R. O. Jakoubek, K. H. Arpag, S. L. Stephens, J. G. Keys, and R. R. Garcia, Visible and near-ultraviolet spectroscopy at McMurdo Station, Antarctica, 10, Reductions of stratospheric NO_2 due to Pinatubo aerosols, *J. Geophys. Res.*, *99*, 3509–3516, 1994.

Thomason, L. W., A diagnostic stratospheric aerosol size distribution, inferred from SAGE II measurements, *J. Geophys. Res.*, *96*, 22,501–22,508, 1991.

Thomason, L. W., Observations of a new SAGE II aerosol extinction mode following the eruption of Mount Pinatubo, *Geophys. Res. Lett.*, *19*, 2179–2182, 1992.

Tolbert, M. A., M. J. Rossi, and D. M. Golden, Heterogeneous interactions of chlorine nitrate, hydrogen chloride, and nitric acid with sulfuric acid surfaces at stratospheric temperatures, *Geophys. Res. Lett.*, *15*, 847–850, 1988.

Tolbert, M. A., J. Pfaff, I. Jayaweera, and M. J. Prather, Uptake of formaldehyde by sulfuric acid solutions: Impact on stratospheric ozone, *J. Geophys. Res.*, *98*, 2957–2962, 1993.

Toohey, D. W., L. M. Avallone, L. R. Lait, P. A. Newman, M. R. Schoeberl, D. W. Fahey, E. L. Woodbridge, and J. G. Anderson, The seasonal evolution of reactive chlorine in the northern hemisphere stratosphere, *Science*, *261*, 1134–1135, 1993.

Treptc, C. R., and M. H. Hitchman, Tropical stratospheric circulation deduced from satellite aerosol data, *Nature*, *355*, 626–628, 1992.

Van Doren, J. M., L. R. Watson, P. Davidovits, D. R. Worsnop, M. S. Zahniser, and C. E. Kolb, Uptake of N_2O_5 and HNO_3 by aqueous sulfuric acid droplets, *J. Phys. Chem.*, *95*, 1684–1689, 1991.

Verdecchia, M., G. Visconti, and G. Pitari, Radiative perturbation due to the eruption of El Chichon: Effect on ozone, *J. Atmos. Terr. Phys.*, *54*, 1081–1084, 1992.

Wilson, J. C., et al., In Situ observations of aerosol and chlorine monoxide after the 1991 eruption of Mount Pinatubo: Effects of reactions on sulfate aerosols, *Science*, *261*, 1140–1142, 1993.

World Meteorological Organization (WMO), Scientific assessment of ozone depletion, *Rep. 20*, Global Ozone Res. and Monit. Proj., U. N. Environ. Programme, Geneva, 1989.

World Meteorological Organization (WMO), Scientific assessment of ozone depletion, *Rep. 25*, Global Ozone Res. and Monit. Proj., U. N. Environ. Programme, Geneva, 1992.

Wuebbles, D. J., D. E. Kinnison, K. E. Grant, and P. S. Connell, Effects of the Mount Pinatubo eruption on the chemistry, radia-

tive, and transport processes in the stratosphere, *Lawrence Livermore Lab Rep., UCRL-JC-111848*, 1993.

P. S. Connell, K. E. Grant, D. E. Kinnison, and D. A. Rotman, Lawrence Livermore National Laboratory, L-262, P.O. Box 808, Livermore, CA 94551. (e-mail: kinnison1@llnl.gov)

D. J. Wuebbles, Atmospheric Science Department, University of Illinois, Urbana, IL 61801.

(Received January 5, 1993; revised July 23, 1994;
accepted August 30, 1994.)